Extended mapping and systematic optimisation of the Carnot battery trilemma for sub-critical cycles with thermal integration

Antoine Laterre[a,b,*], Olivier Dumont[b], Vincent Lemort[b], Francesco Contino[a]

[a] *Institute of Mechanics, Materials and Civil Engineering (iMMC), Université catholique de Louvain (UCLouvain), Place du Levant, 2, Louvain-la-Neuve, 1348, Belgium*
[b] *Thermodynamics Laboratory, University of Liège (ULiège), Allée de la Découverte 17, Liège, 4000, Belgium*

Abstract

Thermally integrated pumped thermal energy storage (TI-PTES) is a flexibility option to recover low-grade heat and provide overnight storage. Common criteria when designing such systems are the power-to-power efficiency (electricity recovery), the exergy efficiency (combined heat and electricity recovery) and the energy density (storage size). However, these are generally conflicting and multi-criteria optimisation is therefore required. Design guidelines have been proposed for some specific case studies but are still lacking for the remaining wide range of possible integrations. This work therefore presents a systematic multi-criteria analysis of a TI-PTES, consisting of a vapour compression heat pump, a sensible heat storage and an organic Rankine cycle, in an extended integration domain. Results show that the storage temperature levels are key variables, as they directly influence the conflict between the performance of the heat pump and the organic Rankine cycle. Also, the intensity of the conflict between the three criteria increases with the temperature difference between the source and the sink, mainly because of the power-to-power efficiency (the density and the exergy efficiency are much less conflicting with each other). Finally, the relevance of thermal integration in TI-PTES is questioned when it leads to a sharp deterioration in exergy efficiency and density.

Keywords:

*Corresponding author.
Email address: `antoine.laterre@uclouvain.com` (Antoine Laterre)

Carnot Battery, Thermally Integrated Pumped Thermal Energy Storage (TI-PTES), Multi-Criteria Optimisation, Performance Mapping, High Temperature Heat Pump, Organic Rankine Cycle

1. Introduction

Next to sufficiency measures, improving the efficiency of energy systems and supporting the integration of renewables are key elements of the energy transition [1]. This includes the deployment of flexibility options, such as energy storage, as well as reducing the amount of energy lost in conversion from one form to another, such as the so-called "waste heat" [2].

Both these points are currently hot topics in the scientific literature. On the one hand, much effort is spent on the development of cost-effective storage systems, like chemical batteries, power-to-x and thermal storage [3]. On the other hand, waste heat is increasingly perceived as an abundant and cheap source of energy [2, 4]. In this regard, it has been estimated that, in 2012, 52% of the primary energy consumed worldwide was actually lost as technically recoverable waste heat [2]. Despite its reduced exergy content (i.e. 63% of this waste energy had a temperature below 100°C, which corresponds to only 21% of the total waste heat exergy content), the challenges of energy transition cannot waste any piece of the enormous volume of energy consumed every year. Another striking figure is that, in EU27, if only about half of the available waste heat were converted into electricity, it is estimated that the equivalent annual production would amount at 150 TWh_{el}/year [5].

There exist several routes to mitigate and recover this waste heat [2]. These include, first, prevention and avoidance, second direct reuse in the process chain (optionally through intermediate heat exchangers), then exergy upgrade with high temperature vapour compression heat pumps (HT-VCHP) [6] and eventually conversion to electricity, using for instance organic Rankine cycles (ORC) [7, 8].

However, there is not always an on-site thermal demand, and the waste heat can have too low exergy potential to make it financially feasible to directly convert it into electricity. In such case, thermally integrated pumped thermal energy storage (TI-PTES, or thermally

Nomenclature

Greek and Latin letters

Δp	pressure losses, bar
ΔT	temperature difference, K
η	efficiency, %
ρ	energy density, kWh/m^3
Ex	exergy, J/kg
h	enthalpy, J/kg
p	pressure, bar
t	temperature, °C
v	specific volume, m^3/kg
W	specific work, J/kg

Sub- and superscripts

cs	cold sink
el	electrical
gl	temperature glide
hp	heat pump
hs	hot source
hs – cs	source - sink temperature
ht	high temperature
II	exergy
lt	low temperature
P2P	power-to-power
pp	pinch point
rel	relative
sc	sub-cooling
sh	super-heating
sp	spread
st	storage

Abbreviations

COP	coefficient of performance
GWP	global warming potential
HP	heat pump
HT-VCHP	high temperature vapour compression heat pump
ODP	ozone depletion potential
ORC	organic Rankine cycle
TES	thermal energy storage
TI-PTES	thermally integrated pumped thermal energy storage

integrated Carnot batteries) could be an alternative option [9]. The latter consists in upgrading the exergy content of a heat source (hotter than the ambient) with excess renewable electricity by using a heat pump, and to store it in a thermal energy storage (TES). Then, when electricity is needed, it can be produced on demand by discharging the TES with a heat engine. TI-PTES is therefore an interesting solution to recover low-grade waste heat while providing the necessary flexibility to renewable energy systems (i.e. energy storage), which gives it more added value and can improve the economic viability of the whole system.

1.1. Thermally integrated pumped thermal energy storage

Since its first mentions by Mercangöz *et al.* [10] and Steinmann [11], and actual first characterisation by Frate *et al.* [9] in 2017, TI-PTES has attracted growing interest and several implementations have been proposed. The most common is the basic hot TI-PTES [12] (depicted in Fig. 1), consisting in a sub-critical HT-VCHP, a two-tank sensible TES and a sub-critical ORC.

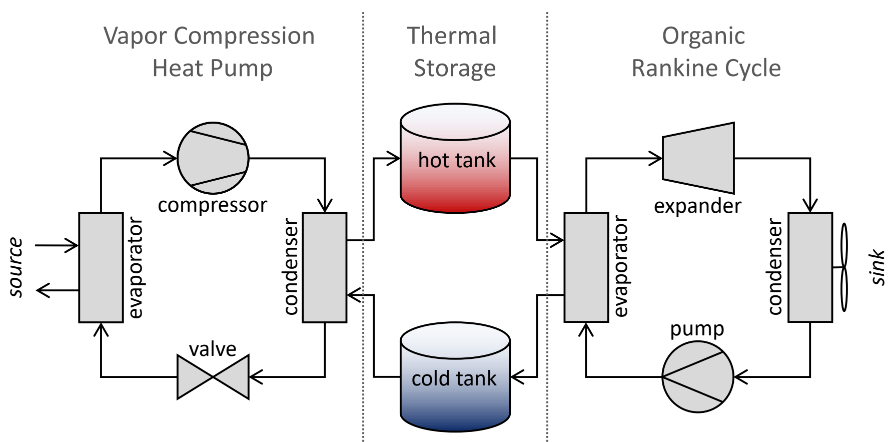

Fig. 1. Layout of the basic hot TI-PTES (Carnot battery). It is composed of a vapour compression heat pump (left), a two-tank sensible heat thermal storage (centre) and an organic Rankine cycle (right). Note that the circulating pumps and other auxiliaries are not shown here.

When optimising the thermodynamic cycle of TI-PTES, typical criteria are to maximise the power-to-power efficiency η_{P2P} (i.e. effectiveness of electricity recovery), the total exergy efficiency η_{II} (i.e. effectiveness of combined heat and electricity recovery) and the electrical energy density ρ_{el} (i.e. storage size). However, as pointed out by Frate *et al.* [12] in the case of a TI-PTES with sensible TES, these three objectives can be conflicting. This implies that it is usually not possible to design a TI-PTES that maximises these criteria simultaneously, and that trade-offs must therefore be discussed. Recently, Weitzer *et al.* suggested to formalise this conflicting nature by referring to it as the *Carnot battery trilemma* [13].

For now, many studies have optimised the thermodynamic design of TI-PTES and proposed cycle modifications to enhance some performance indicators (usually at least η_{P2P}). Frate *et al.* [12, 14] for instance assessed the potential of using internal regenerators in the HT-VCHP and in the ORC. They showed that for source and sink temperatures of 80°C and 15°C respectively, internal regeneration increases η_{II} by 15%, and that it has the potential of being established as the reference configuration for TI-PTES.

Aiming at a better match between the TES and the cycles (thus a better efficiency), and at a higher energy density, Jockenhöfer *et al.* [4] introduced the concept of thermal integration in the CHEST concept [11]. The latter is constructed around an hybrid TES, using both sensible and latent heat storage. On their side, Weitzer *et al.* [13, 15] examined different organic flash cycles for the discharge part. The aim was to reduce the exergy losses during heat transfer between sensible TES with large temperature spreads and the working fluid. They demonstrated for several heat source temperatures that the basic flash cycle did not bring any efficiency enhancement, but that when combined with two-phase expansion and multiple pressure levels, significant efficiency gains were to be expected. They also emphasized that despite their increased complexity, these cycles required further consideration for TI-PTES because of their interesting potential to soften the *Carnot battery trilemma*. Lu *et al.* [16] considered the use of variable composition zeotropic mixtures in the basic TI-PTES configuration to reduce the exergy losses in each exchanger of the HT-VCHP, in addition to the losses between the sensible TES and the discharge cycle. They showed for different heat sink temperatures that interesting gains in η_{II} could be expected.

To continue recovering waste heat while discharging the system, Zhang *et al.* [17] introduced a TI-PTES design where a preheater is inserted into the ORC. This is used to start economising fluid (i.e. preheating the fluid before evaporation) with the waste heat, before evaporation thanks to the heat from the TES. Their analysis showed that for low temperature spreads in the sensible TES, η_{P2P} could increase by more than 15% when the source is at 70°C. Recently, Bellos *et al.* [18] also introduced a new concept based on regenerated cycles and using latent TES, where the waste heat first transfers some of its calories to the TES and then feeds the evaporator of the HT-VCHP with its remaining calories.

Finally, Dumont and Lemort [19] and Xia *et al.* [20] studied an alternative design named "cold TI-PTES". The idea is to use a cold latent TES (generally ice, possibly mixed with other substances to lower the solidification point), in order to increase the energy density without using higher temperature phase change materials, which are logically more expensive than water. A refrigeration cycle is then used to charge the storage tank, releasing the heat from the TES to the ambient. To discharge it, an ORC uses the waste heat as a hot source and the TES as a cold sink. Results showed that despite a lower efficiency than in the hot TI-PTES, the gain in density was non-negligible, which would make it possible to reduce the capital costs. However, more detailed techno-economic analyses are required and it should be noted that, to date, cold TI-PTES has only been treated in a minority of publications.

1.2. Limitations, aims of this study and work novelty

The studies cited above show that sensible heat storage is the most common form of TES in TI-PTES. From a technical point of view, this can be explained by the ease of implementation, and by the lower observed pinches than in latent TES, which is key because Carnot batteries with low-temperature storage ($<$ 150°C) are very sensitive to this parameter [19]. However, this usually comes at the cost of lower energy densities, and less efficient matches between the cycles and the TES. Still, the majority of techno-economic studies also consider sensible TES, generally in two tanks in order to maintain a constant thermal profile and avoid the diffusion problems found in single stratified tanks [12, 21–24].

Although TI-PTES is an active research topic, it should be noted that the majority of studies published to date do not cover the *Carnot battery trilemma* in its entirety. This is reflected in the fact that the technology is often studied in isolation, and not integrated into a specific energy system where all three criteria matter. In particular, the use of waste heat is often perceived as a way of "artificially" boosting η_{P2P}, without looking at the overall energy gain for the energy system in which it is integrated. Density is also frequently overlooked. In addition, many studies are limited to parametric analyses, without any optimisation. Also, although different fluids are sometimes considered, the analysis methods are usually not systematic and therefore do not consider all potential synergies between the fluids and the thermodynamic cycles.

Currently, no paper has focused on optimising and mapping the performance of TI-PTES with respect to the *Carnot battery trilemma* in the entire thermal integration domain (i.e. combination of possible source and sink temperatures). As an illustration, the current domain exploration for TI-PTES with sensible TES is represented in Fig. 2. The region with

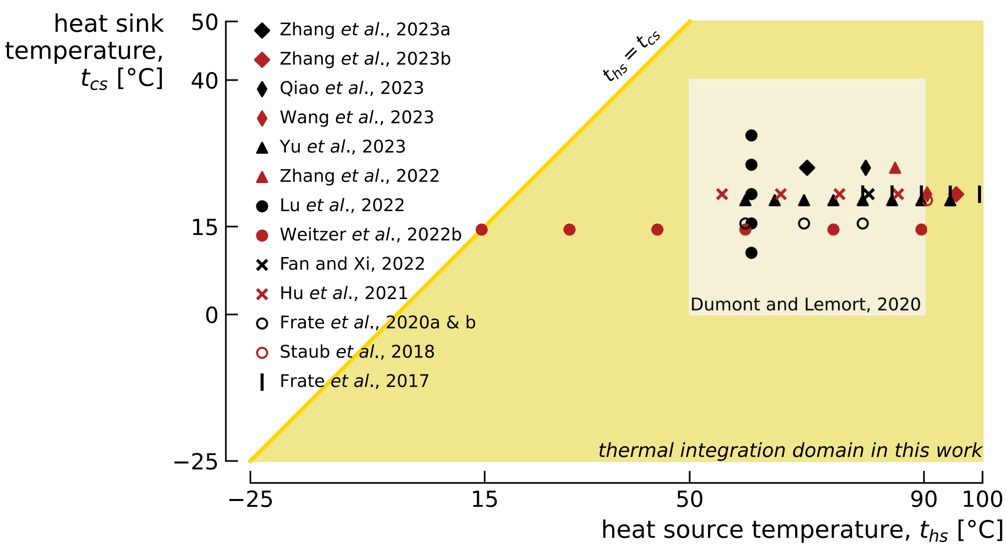

Fig. 2. Current exploration of the thermal integration domain for TI-PTES with sensible TES. Note that most authors have not studied the *Carnot battery trilemma* in its entirety. Moreover, only few of them have conducted proper cycle optimisation. List of references: Zhang *et al.*, 2023a [25]; Zhang *et al.*, 2023b [17]; Qiao *et al.*, 2023 [26]; Wang *et al.*, 2023 [27]; Yu *et al.*, 2023 [24]; Zhang *et al.*, 2022 [23]; Lu *et al.*, 2022 [16]; Weitzer *et al.*, 2022b [15]; Fan and Xi, 2022 [22]; Hu *et al.*, 2021 [21]; Dumont and Lemort, 2020 [19]; Frate *et al.*, 2020a [12] & 2020b [14]; Staub *et al.*, 2018 [28]; Frate *et al.*, 2017 [9].

source temperatures below 60°C has been particularly little explored. This can be attributed in part to the fact that, due to Carnot efficiency, η_{P2P} is lower in that region of the domain (i.e. usually below 50%), whereas as TI-PTES has often been considered primarily as an electrical storage option, this performance may have seemed rather poor. However, when looking at TI-PTES as a flexible waste heat recovery option, there is no indication that η_{P2P} should override η_{II}. Moreover, a significant share (i.e. 45%) of the low temperature waste heat to be recovered (i.e. $<$ 200°C) is precisely below 60°C, as shown by Marina *et al.* [6].

A direct consequence of this poor investigation of the integration domain is that it is currently not possible to provide theoretical maximum performance and design guidelines for TI-PTES across the entire domain, and with regard to the three criteria of the *Carnot battery trilemma*.

The goal of this work is therefore to investigate and characterise the *Carnot battery trilemma* over the entire integration domain. Source temperatures go up to 100°C, a value above which it does not seem appropriate to employ TI-PTES, as waste heat can be recovered more efficiently. The sink temperatures range from -25 to 50°C to cover the majority of climates (i.e. from polar to hot) that can be encountered if the ambience is used as a sink and to represent a certain range of poly-generation applications where the latent heat of condensation in the ORC is recovered.

First, multi-criteria optimisation of the basic hot TI-PTES is conducted to maximise simultaneously the three objectives of the *trilemma*. A specificity of the method is to simultaneously optimise the thermodynamic cycle and the choice of working fluids, to fully embrace the potential synergies between them. Then, the maximum theoretical performance that could be reached is mapped for each objective, and design guidelines are formulated according to the desired objectives. The results are used to assess whether the guidelines can be generalised to the whole domain or whether they need to be adapted in each region. Afterwards, the trilemma is characterised in more details at several relevant locations of the thermal domain. The shape of the Pareto fronts is used to discuss the conflict intensity between the different objectives. Based on the results, implementation constraints are discussed, and design recommendations and cycle improvements are finally proposed.

2. Model and methods

2.1. System model

The system investigated in this work is the basic hot TI-PTES. It consists of a sub-critical HT-VCHP, a two-tank pressurized water TES and a sub-critical air-cooled ORC (see Fig. 1). Although enhanced cycles can give better performance, the basic configuration is adopted as the aim of this study is to provide generic design guidelines for this reference case. Based on the obtained results, cycle improvements are suggested in results section.

The two-tank architecture is preferred to a single tank as it provides a constant thermal profile, regardless of the state of charge and storage duration (i.e. no diffusion losses due to a thermocline). Also, the thermal losses are ignored, so the storage duration has no effect on the tanks temperature. Note that, assuming an ideal thermocline, the results obtained here can be extrapolated to the single tank case [12]. Despite it has a lower energy density, sensible TES is adopted here because latent TES is not mature yet since its thermal stability and reliability remain unclear in the considered temperature range (up to 150°C, see Table 1) [29].

The thermodynamic performance of the system is assessed using `CoolProp` [30] and with an in-house Python model[1] whose parameters are summarised in Table 1. Some are fixed (e.g. pinch-point in heat exchangers) while some others are employed as optimisation variables (e.g. storage temperature). Several constraints are also reported in Table 1. These are employed to give technical plausibility to the cycles and to facilitate their implementation in real machines. For instance, minimum pressures of 0.5 bar are set in the HT-VCHP and in the ORC to limit the necessary degree of vacuum [31]. Of course, above-atmospheric pressures are ideally desired, but this would be quite restrictive for the choice of working fluids in some parts of the domain (the higher the critical point, the lower the saturation

[1]The code can be provided upon request.

pressure, which penalises low saturation temperatures). Also, minimum temperature lifts and drops (i.e. temperature difference between source and sink supplies) of 5 K are set in the HT-VCHP and in the ORC to prevent the cycles from degenerating into configurations where their action on their heat sources would be zero. The hot tank temperature is restricted to 150°C to limit the need for water pressurisation (thus the cost) and the maximum compressor discharge temperature is 180°C to represent the current HT-VCHP practice [32–34]. Main reasons for that are to prevent lubricant degradation and fluid decomposition [31].

Table 1

Model parameters and constraints for the TI-PTES optimisation.

Name	**Symbol**	**Value**	**Name**	**Symbol**	**Value**
Heat source temperature	t_{hs}	-25 to 100°C	Heat sink temperature	t_{cs}	-25 to 50°C
Heat source temp. glide	$\Delta T_{hs,gl}$	*design var.*	Heat sink temp. glide	$\Delta T_{cs,gl}$	10 K [12]
HP vapour super-heating	$\Delta T_{hp,sh}$	*design var.*	ORC vapour super-heating	$\Delta T_{orc,sh}$	*design var.*
HP liquid sub-cooling	$\Delta T_{hp,sc}$	*design var.*	ORC liquid sub-cooling	$\Delta T_{orc,sc}$	3 K [13]
Min. HP temperature lift	ΔT_{hp}^{min}	5 K [19]	Min. ORC temp. drop	ΔT_{orc}^{min}	5 K [19]
HP working fluid	$fluid_{hp}$	*design var.*	ORC working fluid	$fluid_{orc}$	*design var.*
Compressor efficiency	$\eta_{is,comp}$	0.75 [19]	Expander efficiency	$\eta_{is,exp}$	0.75 [19]
Max. compress. exit temp.	t_{hp}^{max}	180°C [12]	Pump efficiency	$\eta_{is,pmp}$	0.50 [19]
Min. HP/ORC super-heating	ΔT_{sh}^{min}	3 K [13]	Min. HP sub-cooling	ΔT_{sc}^{min}	3 K [13]
Hot tank storage temp.	$t_{st,ht}$	*design var.*	Storage temp. spread	$\Delta T_{st,sp}$	*design var.*
Max. storage temperature	$t_{st,ht}^{max}$	150°C [13]	Storage pressure	p_{st}	7.5 bar
Min. storage temperature	$t_{st,lt}^{min}$	$t_{hs} - \Delta T_{hs,gl}$	Min. HP/ORC pressure	$p_{hp/orc}^{min}$	0.5 bar [12]
Pinch point in exchangers	ΔT_{pp}	3 K [12, 19]	Pressure losses	Δp	0.0 bar [12, 13]

In this model, the evaporation and condensation pressures are obtained with the pinch method. Unlike Frate *et al.* [12], who imposed a minimum pinch temperature difference while allowing their model to use higher ones, this approach is selected to reduce the number of design variables (the saturation pressures in the HT-VCHP and in the ORC are here fixed by the temperature profile of the secondary fluids), which relaxes the optimisation problem. This is also justified by the fact that most studies have shown that the pinch point must be as low as possible to maximise the efficiency [15, 19].

Another assumption is that all pressure drops, which are technology dependent, are neglected to get more generic conclusions. Nevertheless, the sensitivity of TI-PTES performance to these losses deserves further analyses. Also note that the heat source and sink are treated as pure dry atmospheric air (i.e. only sensible heat is considered, no humidity).

2.2. Optimisation problem

The *Carnot battery trilemma* consists of the conflict between the power-to-power efficiency η_{P2P}, the exergy efficiency η_{II}, and the energy density ρ_{el}. These performance indicators are therefore adopted for the multi-criteria optimisation. They are defined as

$$\eta_{\mathrm{P2P}} = \frac{\mathrm{W_{orc}}}{\mathrm{W_{hp}}} \,, \tag{1}$$

$$\eta_{\mathrm{II}} = \frac{\mathrm{W_{orc}}}{\mathrm{W_{hp}} + \mathrm{Ex_{hs}}} \,, \tag{2}$$

$$\rho_{\mathrm{el}} = \frac{\mathrm{h_{st,ht}} - \mathrm{h_{st,lt}}}{\mathrm{v_{st,ht}} + \mathrm{v_{st,lt}}} \cdot \eta_{\mathrm{orc}} \,, \tag{3}$$

where $\mathrm{W_{orc}}$ and $\mathrm{W_{hp}}$ are the ORC and HT-VCHP net work output and input, respectively, and $\mathrm{Ex_{hs}}$ is the exergy of the heat source. The reference state used for the latter's definition corresponds to the heat sink temperature. The specific case $\mathrm{t_{hs}} = \mathrm{t_{cs}}$ thus yields $\eta_{\mathrm{II}} = \eta_{\mathrm{P2P}}$, since $\mathrm{Ex_{hs}} = 0$. The density corresponds to the amount of electricity that can be discharged per unit volume of the tanks.

To optimise the performance of TI-PTES, a set of eight design variables are used. The hot tank storage temperature $\mathrm{t_{st,ht}}$, the heat source glide $\Delta\mathrm{T_{hs,gl}}$ (i.e. temperature difference between supply and exit of the evaporator of the HT-VCHP) and the storage temperature spread $\Delta\mathrm{T_{st,sp}}$ (i.e. temperature difference between the hot and cold tanks) have already been identified as key parameters influencing η_{P2P}, η_{II} and ρ_{el} respectively [12, 15, 19]. Note that it is here assumed that the heat source can be treated as "free" waste heat (i.e. the heat source glide has no constrained value and is therefore used as a design variable). We also include the liquid sub-cooling $\Delta\mathrm{T_{hp,sc}}$ in the HT-VCHP as well as the vapour superheating $\Delta\mathrm{T_{hp/orc,sh}}$ in the HT-VCHP and in the ORC. Indeed, these parameters can take different optimum values depending on the thermal profiles and working fluids [12, 35]. The constraints associated with these variables are reported in Table 1.

Finally, an innovative aspect of the method proposed here compared with the state of the art in Carnot battery research is to simultaneously optimise the thermodynamic cycle and the selection of working fluids in the HT-VCHP and ORC, to fully embrace the existing synergies between them (instead of running optimisation for all possible pairs and keeping only the best performing sets [14]). In this work, a list of 34 working fluids is considered. These were selected from the list of those available in `CoolProp` because they have zero ozone depletion potential (compliance with Montreal protocol), low to moderate global warming potential (compliance with Kigali Amendment and EU F-gas regulation) and because their critical point is compatible with sub-critical cycles in the temperature range investigated in this work (i.e. thermal domain and storage temperatures). The full list of fluids is available in Table 2.

To map the performance of TI-PTES, the integration domain is discretised with a 5 K resolution into 296 cells. In each cell, optimisation is carried out using NSGA-II [37], a well established genetic algorithm for multi-criteria problems, through the `RHEIA` framework [38]. Note that particle swarm optimisation was also tested through `pymoo` [39]. However, it did not show a lower computational budget for equivalent optima.

In Table 1, all design variables are continuous except the working fluids. To integrate them to the problem, these were sorted by critical temperature and got assigned tags ranging from 1 to 34. The continuous design space for each fluid then ranges from 0.51 to 34.49, and each tag is obtained by converting the value to the closest integer. Note that sorting the fluid by critical temperature is intended to facilitate the natural selection of well performing fluids from generation to generation.

The optimisation process was carried out in two main stages, in order to achieve global convergence and avoid the curse of local optima. Indeed, the optimisation domain to be covered is relatively complex - the term porous could be employed - as many combinations

Table 2

Technical and physical properties of the investigated working fluids (data from CoolProp 6.4.1 [30]).

Fluid	Type	T_{crit} [°C]	p_{crit} [bar]	$p_{sat,15°C}$ [bar]	GWP_{100}	ASHRAE 34[b]	Shape	No.
R1150 (Ethylene)	HO	9.2	50.4	n.a.	6.8	A3	wet	1
R170 (Ethane)	HC	32.2	48.7	33.7	0.437[a]	A3	wet	2
R41	HFC	44.1	59.0	30.1	135[a]	N/A	wet	3
R1270 (Propylene)	HO	91.1	45.6	8.9	3.1	A3	wet	4
R1234yf	HFO	94.7	33.8	5.1	0.501[a]	A2L	dry	5
R290 (Propane)	HC	96.7	42.5	7.3	0.02[a]	A3	wet	6
R161	HFC	102.1	50.1	7.0	4.84[a]	N/A	wet	7
R1243zf	HFO	103.8	35.2	4.4	0.261[a]	N/A	isentropic	8
R1234ze(E)	HFO	109.4	36.3	3.6	1.37[a]	A2L	isentropic	9
R152a	HFC	113.3	45.2	4.4	164[a]	A2	wet	10
R13I1	H	123.3	39.5	3.7	0.4	A1	wet	11
RC270 (cyclo-Propane)	HC	125.2	55.8	5.5	N/A	A3	wet	12
RE170 (dimethyl-Ether)	HC	127.2	53.4	4.4	1.0	A3	wet	13
R717 (Ammonia)		132.2	113.3	7.3	N/A	B2L	wet	14
R600a (iso-Butane)	HC	134.7	36.3	2.6	N/A	A3	dry	15
1-Butene	HC	146.1	40.1	2.2	N/A	N/A	dry	16
R1234ze(Z)	HFO	150.1	35.3	1.2	0.315[a]	A2L	isentropic	17
R600 (n-Butane)	HC	152.0	38.0	1.8	0.006[a]	A3	dry	18
trans-2-Butene	HC	155.5	40.3	1.7	N/A	N/A	dry	19
Neopentane	HC	160.6	32.0	1.2	N/A	N/A	dry	20
R1233zd(E)	HCFO	166.5	36.2	0.9	3.88[a]	A1	dry	21
Novec649		168.7	18.7	0.3	N/A	N/A	dry	22
R601a (iso-Pentane)	HC	187.2	33.8	0.6	N/A	A3	dry	23
R601 (n-Pentane)	HC	196.5	33.7	0.5	N/A	A3	dry	24
R602 (n-Hexane)	HC	234.7	30.4	0.1	3.1	N/A	dry	25
Acetone		235.0	47.0	0.2	0.5	N/A	isentropic	26
cyclo-Pentane	HC	238.6	45.7	0.3	N/A	N/A	dry	27
Methanol		239.4	82.2	0.1	2.8	N/A	wet	28
R603 (n-Heptane)	HC	267.0	27.4	< 0.1	N/A	N/A	dry	29
cyclo-Hexane	HC	280.5	40.8	< 0.1	N/A	N/A	dry	30
Benzene	HC	288.9	48.9	< 0.1	N/A	N/A	dry	31
MDM	Siloxane	290.9	14.1	< 0.1	N/A	N/A	dry	32
Toluene	HC	318.6	41.3	< 0.1	3.3	N/A	dry	33
ethyl-Benzene	HC	344.0	36.2	< 0.1	N/A	N/A	dry	34

[a] Value from Table 7.SM.7 of IPCC AR6 [36]

[b] ASHRAE Standard 34-2022, "Designation and Safety Classification of Refrigerants"

of variables lead to physically infeasible solutions or which do not respect the design constraints (e.g. high storage temperatures make sub-critical operations impossible if the critical temperature of the fluid is too low). To cover this domain properly, the population size and mutation probability are first set to 500 and 50%, respectively. In this sense, the idea is to build a preliminary map in a way that is almost like a random search. Experience has shown that a number of 1000 generations is generally sufficient to obtain "global" optima for each objective. The results are then post-processed: when a cell of the thermal domain shows much worse performance than its neighbours or causes a discontinuity in the map trends, some individuals from the surrounding cells are inserted in its population. Then, optimisation is relaunched for that cell. In a second time, the mutation probability is reduced to 10% and optimisation is relaunched in the entire domain to refine the results. These two steps are reproduced until a global convergence seems to be reached (without any guarantee) and uniformity is obtained on the performance map. The optimisation process is illustrated in Fig. 3.

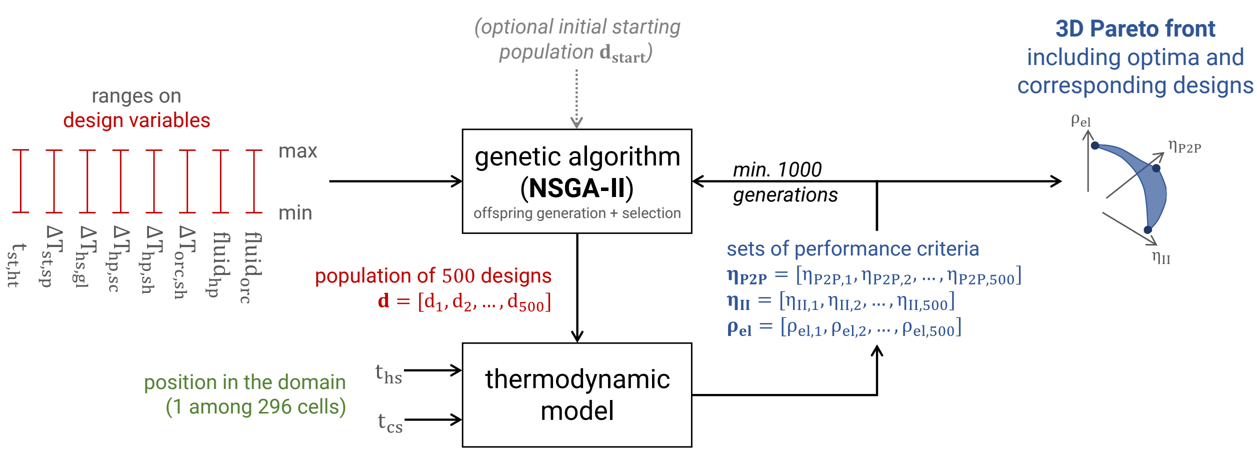

Fig. 3. Illustration of the optimisation process carried out in each cell. Initially, no starting population is provided, so the optimiser selects the 500 designs from the ranges of design variables through Latin Hypercube Sampling. A set of 1000 generations is then run with a mutation probability of 50% to capture the global optima. In a second step, the mutation probability is reduced to 10% and the optimisation is relaunched using the last generation as initial starting population. This refines the results and smoothes the Pareto front.

3. Results

The first part of the results focuses on mapping the performance of TI-PTES over the entire thermal integration domain, and on analysing the optimal thermodynamic designs. The various trends are then discussed and design guidelines are step by step constructed according to the objectives sought. Conflicts between the different objectives are also qualitatively illustrated by juxtaposing the different maps in a pay-off table. In the second part, the design guidelines are summarised and graphically illustrated over the domain. Further discussions on some design parameters are also carried out. In the third part, the *Carnot battery trilemma* is studied quantitatively by analysing the Pareto fronts resulting from the multi-criteria analysis. A conflict index is also set up to map the intensity of the *trilemma.*

3.1. Performance mapping

In each of 296 the cells of the domain (i.e. combination of source and sink temperatures), the three designs providing the best η_{P2P}, η_{II}, and ρ_{el} were selected to construct the maps. These are depicted in Fig. 4. They are represented as a pay-off table to illustrate the conflict between the different objectives of the *trilemma*: for each optimised objective, the value of the two others is also mapped. Since they are key variables in TI-PTES [12, 19], the corresponding heat source temperature glide $\Delta \mathrm{T}_{\mathrm{hs,gl}}$, hot storage temperature $\mathrm{t}_{\mathrm{st,ht}}$ and storage temperature spread $\Delta \mathrm{T}_{\mathrm{st,sp}}$ are depicted in Fig. 5. The other design variables, including the working fluids, vapour super-heating and liquid sub-cooling are discussed later in Section 3.2. Finally, in order to make the thermodynamic cycles more legible and complementary to the maps, typical T-s diagrams are shown in Fig. A.1 in Appendix A.

3.1.1. Results for optimised η_{P2P}

As illustrated in Fig. 4, the power-to-power efficiency increases with the difference between the source and sink temperatures $\Delta \mathrm{T}_{\mathrm{hs-cs}}$ from about 30% when $\Delta \mathrm{T}_{\mathrm{hs-cs}} = 0$ K to about 440% when $\Delta \mathrm{T}_{\mathrm{hs-cs}} = 125$ K. However, because of a design shift, the growth is not continuous (the tipping point is $\Delta \mathrm{T}_{\mathrm{hs-cs}} = 30$ K). Indeed, for $\Delta \mathrm{T}_{\mathrm{hs-cs}} > 30$ K, the hot storage temperature $\mathrm{t}_{\mathrm{st,ht}}$ is minimised so that the heat pump lift $\Delta \mathrm{T}_{\mathrm{hp}}$ (i.e. the temperature

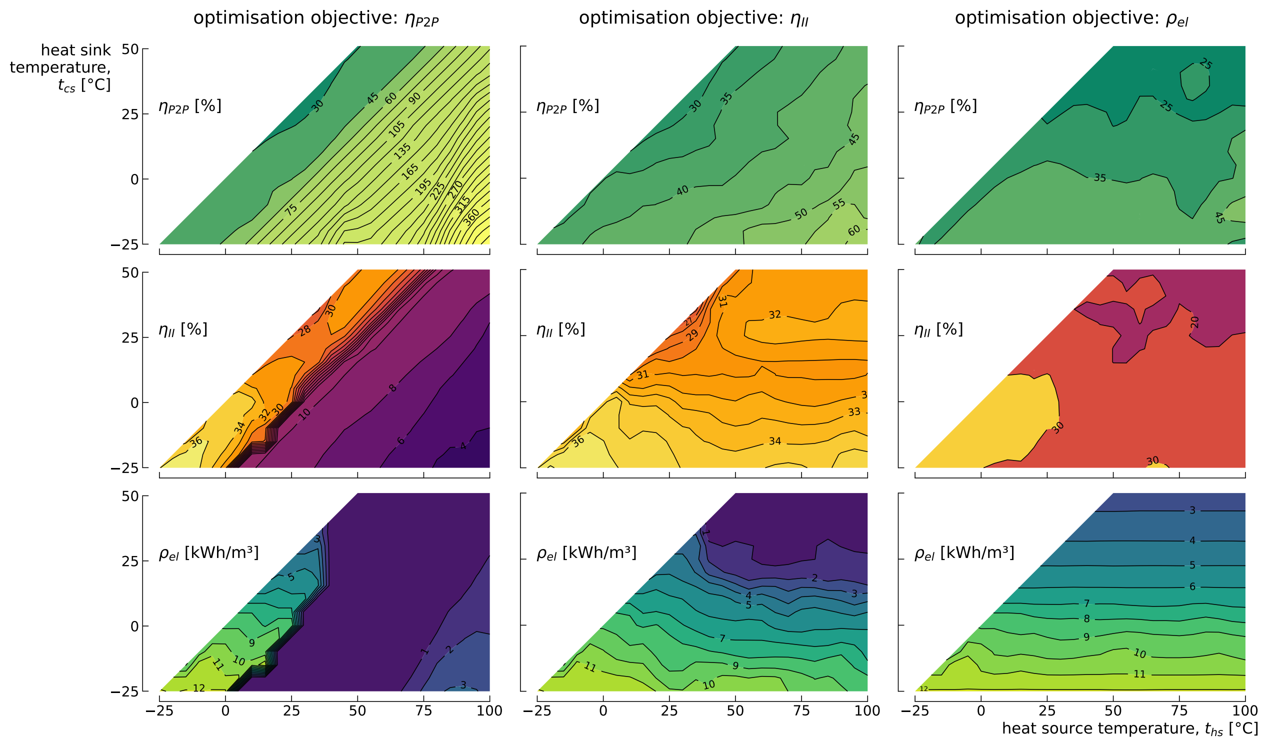

Fig. 4. Performance maps with η_{P2P} (1st row), η_{II} (2nd row) and ρ_{el} (3rd row) for the configurations maximising η_{P2P} (1st column), η_{II} (2nd column) and ρ_{el} (3rd column), respectively. Some maps have been smoothed using Gaussian filtering to eliminate local convergence issues (model artefacts). Please note that the spacing between the contour lines is refined on some maps to increase legibility.

difference between the storage and the source, $\mathrm{t_{st,ht}} - \mathrm{t_{hs}}$) is always minimised. In this sense, the coefficient of performance of the HT-VCHP is maximised to the detriment of the ORC efficiency, which is affected by the lower $\mathrm{t_{st,ht}}$.

The existence of the 30 K tipping point, which had also been observed by Weitzer *et al.* [15], can be explained with $\eta_{\mathrm{P2P}}^{\mathrm{Carnot}}$, the Carnot efficiency of TI-PTES (i.e. the thermodynamic limit) [4]. Considering the irreversibilities at the heat transfers between the working fluids and the secondary fluids, which can be modelled as the temperature difference $\Delta\mathrm{T}$ between the fluids (comparable to a pinch temperature), and assuming endoreversible HT-VCHP and ORC (i.e. no internal irreversibilities), the latter is defined as

$$\eta_{\mathrm{P2P}}^{\mathrm{Carnot}} = \mathrm{COP}_{\mathrm{hp}}^{\mathrm{Carnot}} \cdot \eta_{\mathrm{orc}}^{\mathrm{Carnot}} = \frac{\mathrm{t_{st,ht}} + \Delta\mathrm{T}}{\mathrm{t_{st,ht}} - \mathrm{t_{hs}} + 2\Delta\mathrm{T}} \cdot \frac{\mathrm{t_{st,ht}} - \mathrm{t_{cs}} - 2\Delta\mathrm{T}}{\mathrm{t_{st,ht}} - \Delta\mathrm{T}} \quad , \tag{4}$$

and it is depicted in Fig. 6. When $\Delta\mathrm{T_{hs\text{--}cs}}$ is below the tipping point (i.e. $\Delta\mathrm{T_{hs\text{--}cs}} < 30$

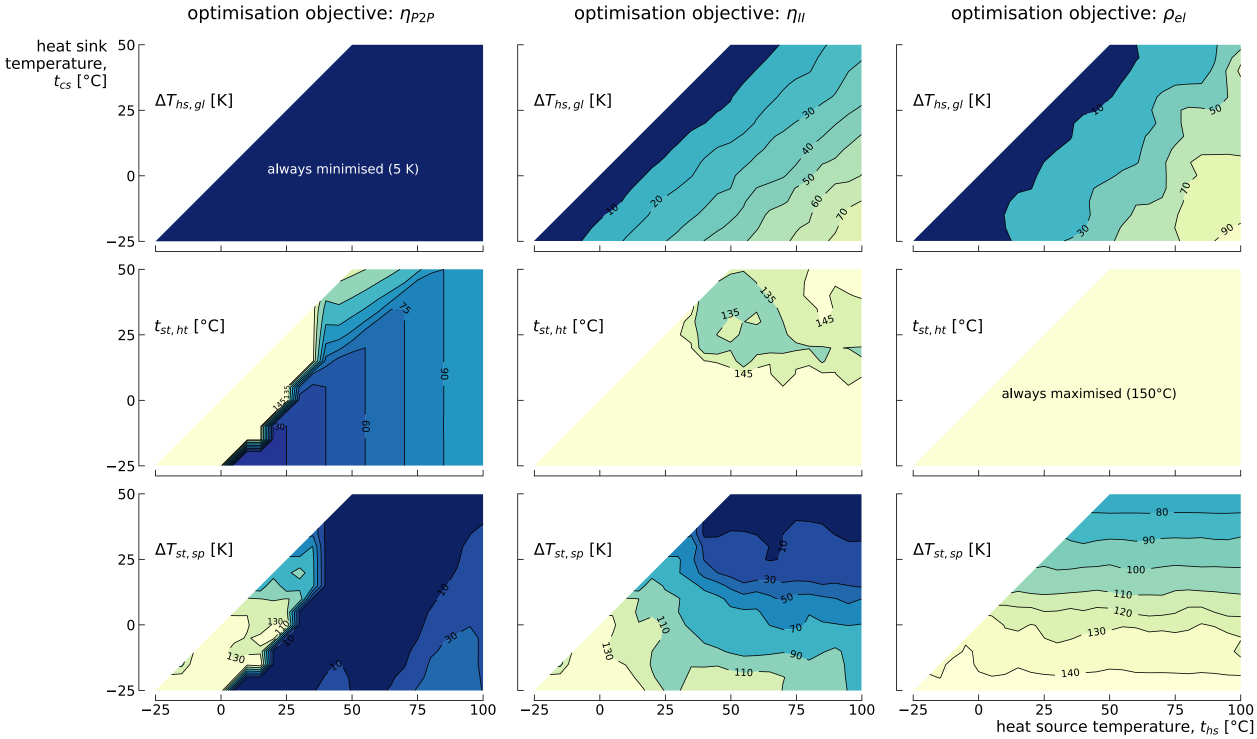

Fig. 5. Set of design variables with the most significant influence on the Carnot battery trilemma: $\Delta T_{hs,gl}$ (1st row), $t_{st,ht}$ (2nd row) and $\Delta T_{st,sp}$ (3rd row). Some contour lines have been smoothed to eliminate local convergence issues (model artefacts).

K for $\Delta T = 8$ K), the exergy losses at the ORC cannot be sufficiently compensated by the high COP, thus $t_{st,ht}$ must be increased to reduce these losses and to increase η_{orc}, so that the resulting η_{P2P} is improved (see Fig. 6a).

It can also be shown that the tipping point increases with the heat transfer irreversibilities (see difference between $\Delta T = 0$ and 8 K in Fig. 6). Note that the particular case $\Delta T = 0$ (i.e. no irreversibilities) does not allow detection of the tipping point, and therefore leads to incorrect conclusions about the optimum $t_{st,ht}$ (Fig. 6b illustrates that minimising $t_{st,ht}$ is always beneficial). Also note that this "30 K" value is specific to the pinch-point selected in this work. Furthermore, as the charging and discharging cycles are not endoreversible (there are internal irreversibilities due, among others, to the compression and expansion machines), it cannot be said that it is solely a function of heat transfer irreversibilities. However, 30 K seems to be the value to bear in mind for TI-PTES since Weitzer *et al.* [15] obtained a

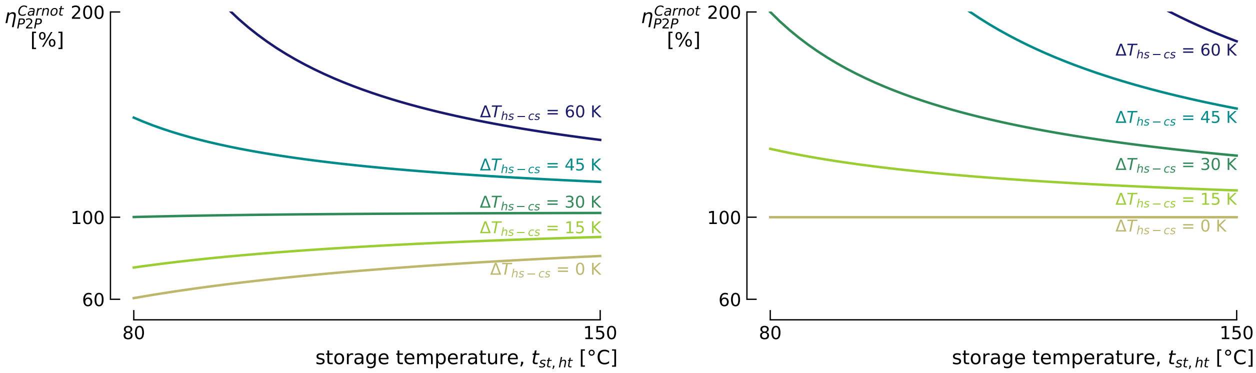

(a) Cold sink: $t_{cs} = 20°C$, irreversibilities: $\Delta T = 8$ K

(b) Cold sink: $t_{cs} = 20°C$, irreversibilities: $\Delta T = 0$ K

Fig. 6. Carnot efficiency of TI-PTES with and without consideration of heat transfer irreversibilities. The latter are represented through ΔT, the temperature difference between the working fluids and the secondary fluids. It illustrates well that a TI-PTES model which ignores the heat transfer irreversibilities does not allow to detect the tipping point and always recommends to minimise $t_{st,ht}$.

similar value comprised between 25 K and 40 K.

Below the tipping point (i.e. $\Delta T_{hs-cs} \leq 30$ K), on the other hand, the lift is almost always maximised, so $t_{st,ht} = t_{st,ht}^{max} = 150°C$ in that region of the domain. The only exception is for the part $t_{hs} > 35°C$ and $\Delta T_{hs-cs} \leq 30$ K, where $t_{st,ht}$ gradually increases with decreasing ΔT_{hs-cs}. The reason for this discontinuity in $t_{st,ht}$ is due to the constraint $t_{st,ht}^{max} = 150°C$. In fact, as t_{cs} is also higher in that region, η_{orc} is penalised since the difference $t_{st,ht} - t_{cs}$ decreases. To compensate, COP_{hp} is increased by reducing $t_{st,ht}$ (which, by the way, affects η_{orc} even more). An optimum trade-off must therefore be found between η_{orc} and COP_{hp}. Note that the existence of this zone is purely due to the technological constraint on $t_{st,ht}^{max}$. In fact, by increasing the latter, η_{orc} would increase again and it would no longer be necessary to decrease $t_{st,ht}$ to maximise η_{P2P}. This is illustrated for one cell of the domain in Appendix B by raising $t_{st,ht}^{max}$ to 200°C, although this is probably beyond the current technological limits for HT-VCHP. The message that emerges from this analysis is thus that the optimum thermodynamic configuration is a function of the design constraints.

Note that the analysis with η_{P2P}^{Carnot} tends to validate the assumption that $t_{st,ht}$ should always be maximised below the tipping point (even for $t_{hs} > 35°C$), and that the results observed in Fig. 5 are effectively due to the constraint on $t_{st,ht}^{max}$.

Finally, it should be noted that the loss in η_{P2P} due to this $t_{st,ht}^{max} = 150°C$ constraint is very small. In fact, the iso-η_{P2P} lines shown in Fig. 4 are homogeneous in this region of the domain and show no discontinuity. On the other hand, it can be seen that the spread is minimised there, resulting in a significant reduction in ρ_{el}.

Overall, this analysis perfectly illustrates that approaches such as near-optimum analyses [40] can lead to different designs for similar performance, and that such methods should be considered, for instance, to identify whether tolerating a small loss in η_{P2P} makes it possible to maintain ρ_{el} at a high level. This issue is further discussed in the multi-criteria analysis in Section 3.3.

Another key message from these results is that, when ΔT_{hs-cs} is above the tipping point, the search for the maximum η_{P2P} leads to a TI-PTES degenerated into a TES + ORC (i.e. the heat pump lift is minimised), which makes it a waste heat recovery option, but no longer a true electrical storage system. This observation has very practical consequences. When the TI-PTES is used with free waste heat (heat source glide not constrained by the application) in this part of the domain, the sole search for the best η_{P2P} is an absurdity because it leads to the use of an HT-VCHP whose action is zero: the exergy content of the waste heat is not increased (i.e. the thermal storage is at the same temperature as the source) and the electrical consumption of the HT-VCHP then turns out to be pure exergy destruction. This degeneration is well illustrated in the T-s diagrams in Figs. A.1g & A.1j in Appendix A: the HT-VCHP only raises the $t_{st,ht}$ by 5 K compared with the t_{hs} (minimum constraint), and the extent of exergy loss through the heat transfers is clearly visible.

Regarding the other two design variables, since maximising η_{P2P} involves getting as close as possible to ideal Carnot cycles, the heat source glide $\Delta T_{hs,gl}$ and storage temperature spread $\Delta T_{st,sp}$ are minimised on the largest part of the domain to limit the exergy losses at the heat transfers, and to get close to square shapes on the T-s diagrams (see Figs. A.1d &

A.1g). Consequently, η_{II} and ρ_{el} are rather poor (see Fig. 4), since a lot of exergy is lost at the source ($\Delta\mathrm{T}_{\mathrm{hs,gl}}$ is minimised) and because the low $\Delta\mathrm{T}_{\mathrm{st,sp}}$ limits the thermal density. It should be noted, however, that η_{II} gradually deteriorates as $\Delta\mathrm{T}_{\mathrm{hs-cs}}$ increases, because the exergy content of the source also increases, while most of it is lost to the environment (because the heat source glide is low). The minimisation of $\Delta\mathrm{T}_{\mathrm{st,sp}}$ is in line with the results reported by Weitzer *at al.* [15]: they showed that for storage temperatures below 120°C, increasing $\Delta\mathrm{T}_{\mathrm{st,sp}}$ deteriorates η_{P2P}.

Let us also mention that in the south-eastern part of the domain, $\Delta\mathrm{T}_{\mathrm{st,sp}}$ increases slightly (this is also visible in Fig. 7 where $\Delta\mathrm{T}_{\mathrm{hs-cs}} > 60$°C) in order to reduce the condensation temperature in the HT-VCHP (see Fig. A.1j) and to increase its COP, which results in a partial improvement in the density.

The above analysis does however not apply to the region of the domain where the storage temperature is maximised (i.e. below the 30 K tipping point). There, the storage spread takes much higher values: the relative storage spread, which is defined as

$$\Delta\mathrm{T}_{\mathrm{st,sp}}^{\mathrm{rel}} = \frac{\Delta\mathrm{T}_{\mathrm{st,sp}}}{\mathrm{t}_{\mathrm{st,ht}} - \mathrm{t}_{\mathrm{cs}}} \quad , \tag{5}$$

lies between 50% and 90% as illustrated in Fig. 7. Weitzer *et al.* [15] also showed that when the storage temperature was maximised, increasing the storage temperature spread to an optimum value was necessary to maximise η_{P2P}. The main reason for this is that large spreads make it possible to lower the condensation temperature in the HT-VCHP, which reduces the compression work, while at the same time allowing significant sub-cooling, which increases the refrigeration effect, thus improving the COP (this is well illustrated by the T-s diagram in Fig. A.1a). However, as this penalises the ORC efficiency, there is an optimal spread to be found. Interestingly, this leads to increased ρ_{el} and relaxes the *Carnot battery trilemma*, as this will be further discussed in the multi-criteria analysis.

To ease the formulation of guidelines, Fig. 7 also introduces the relative heat pump lift,

$$\Delta\mathrm{T}_{\mathrm{hp}}^{\mathrm{rel}} = \frac{\mathrm{t}_{\mathrm{st,ht}} - \mathrm{t}_{\mathrm{hs}}}{\mathrm{t}_{\mathrm{st,ht}}^{\mathrm{max}} - \mathrm{t}_{\mathrm{hs}}} \quad . \tag{6}$$

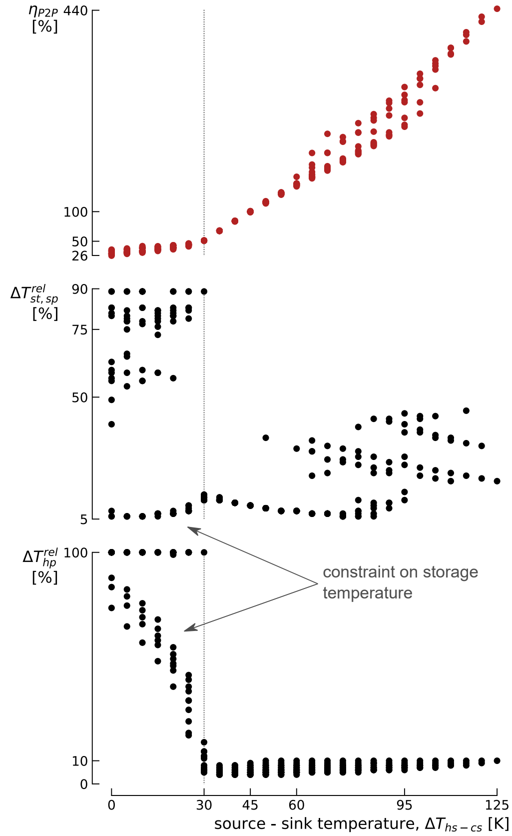

Fig. 7. Optimised power-to-power efficiency (red dots), corresponding relative storage spread $\Delta T^{rel}_{st,sp}$ (black dots) and corresponding relative heat pump lift ΔT^{rel}_{hp} (black dots) depicted according to their source - sink temperatures. The deviation from theory due to $t^{max}_{st,ht} = 150°C$ is clearly visible for $\Delta T^{rel}_{st,sp}$ and ΔT^{rel}_{hp}.

The latter clearly shows where the lift is minimised and maximised, and prescribes it a value in the region where $\Delta T_{hs-cs} \leq 30$ K and $t_{hs} > 35°C$ (region which exists because of the constraint on the maximum storage temperature).

3.1.2. Results for optimised η_{II}

The exergy efficiency globally drops as the sink temperature t_{cs} increases from about 36% when $t_{cs} = -25°C$ to about 30% when $t_{cs} = 15°C$ (see Figs. 4 & 8). The main driver is the decrease of the ORC efficiency η_{orc} (see Fig. 8). This is because, in that region of the domain, the storage temperature $t_{st,ht}$ is always maximised (i.e. maximisation of η_{orc} to the cost of reduced COP_{hp}), so that, by Carnot efficiency, an increase in t_{cs} leads to a reduction

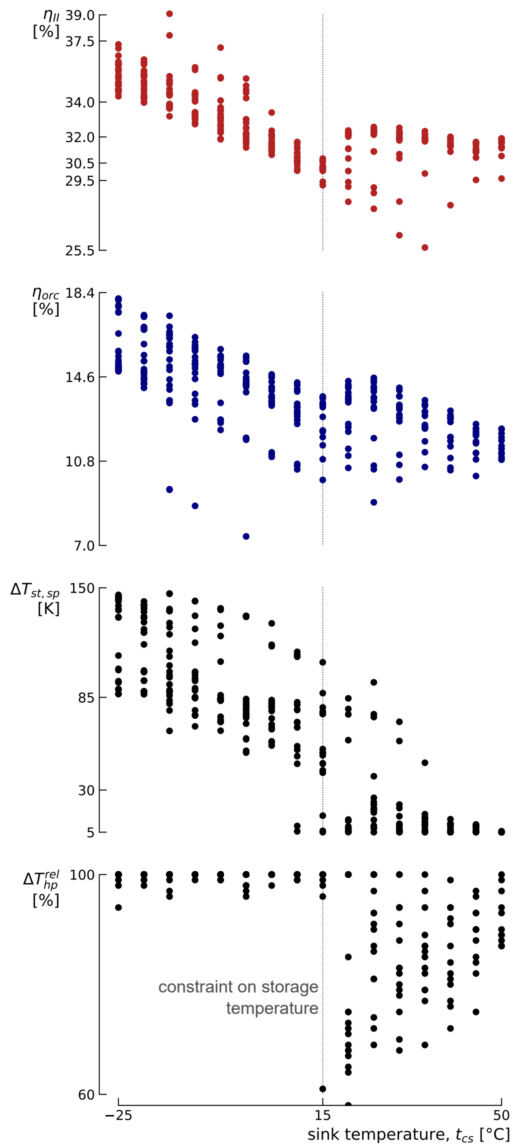

Fig. 8. Optimised exergy efficiency (red dots), ORC efficiency (blue dots), storage temperature spread (black dots) and corresponding relative heat pump lift (black dots) depicted according to the sink temperatures.

in η_{orc}. Also note that the storage temperature spread $\Delta T_{st,sp}$ decreases as t_{cs} increases, so as not to affect η_{orc} too much. Indeed, for some $t_{st,ht}$ and t_{cs}, the greater the spread, the lower the evaporation point, and therefore the lower η_{orc}.

This result is partly in contrast with that of Frate *et al.* [12] who, for equivalent design variables, also recommended maximising $t_{st,ht}$ but minimising $\Delta T_{st,sp}$ to maximise η_{II}. The explanation we find is that, when $t_{st,ht}$ is maximised, increasing the spread is necessary because the gain in COP due to sub-cooling in the HT-VCHP compensates for the loss in η_{orc} (i.e. there is an optimum trade-off between COP_{hp} and η_{orc}).

When $t_{cs} > 15$°C, η_{II} slightly re-increases and stabilises around 32% because of a design shift (see Fig. 8): $t_{st,ht}$ is reduced to values between 130°C and 150°C (especially for lower ΔT_{hs-cs}) and $\Delta T_{st,sp}$ to values below 30 K. The reason for this shift is the same as the one introduced for η_{P2P}: while η_{orc} deteriorates and cannot be increased by a higher $t_{st,ht}$ because of the $t^{max}_{st,ht}$ constraint, it can no longer compensate for the lower COP_{hp}. Reducing $t_{st,ht}$ slightly therefore helps to find the right balance between η_{orc} and COP_{hp}. Finally, the drop in ΔT_{hs-cs} increases η_{orc} for the same reasons as given above (this is clearly visible in Fig. 8).

The other key parameter influencing η_{II} is the heat source glide $\Delta T_{hs,gl}$. A high $\Delta T_{hs,gl}$ leads to an effective waste heat utilisation (it reduces the exergy losses at the source) but reduces COP_{hp} as the evaporation temperature is decreased (the heat source temperature at the evaporator outlet is lower, see Figs. A.1h & A.1k). A trade-off must therefore be found. The relative heat source glide, defined as

$$\Delta T^{rel}_{hs,gl} = \frac{\Delta T_{hs,gl}}{\Delta T_{hs-cs}} \quad , \tag{7}$$

remains between 50 and 60% when η_{II} is maximised (see Fig. 9).

Finally, it should be noted that because $\Delta T_{st,sp}$ is relatively high there, the density ρ_{el} obtained throughout the zone where $t_{st,ht} = 150$°C when η_{II} is maximised is close to that obtained when ρ_{el} is maximised (see third column in Fig. 4). This will be further discussed in the multi-criteria analysis, in Section 3.3.

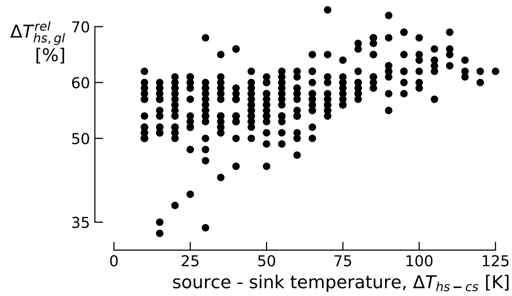

Fig. 9. Relative heat source glide for the design maximising the exergy efficiency.

3.1.3. Results for optimised ρ_{el}

The optimum electrical energy density is a trade-off between the thermal density (i.e. the higher $\Delta T_{\mathrm{st,sp}}$, the higher the thermal density) and η_{orc} (i.e. the higher $\Delta T_{\mathrm{st,sp}}$, the lower η_{orc}). As it can be observed in Figs. 4 & 10, because η_{orc} is a function of t_{cs}, ρ_{el} linearly decreases with increasing t_{cs}. It ranges from 12.3 kWh/m^3 when $t_{\mathrm{cs}} = -25$°C to 2.5 kWh/m^3 when $t_{\mathrm{cs}} = 50$°C. Note that a TES in a single tank with an ideal thermocline could double these values, as one of the two tanks would be removed.

The optimum storage spread linearly varies from about 150 K when $t_{\mathrm{cs}} = -25$°C to about 70 K when $t_{\mathrm{cs}} = 50$°C. To reach such spreads and to maximise η_{orc}, $t_{\mathrm{st,ht}}$ is always maximised. Moreover, as a rule of thumb, it is shown in Fig. 10 that for the designs maximising the density, $t_{\mathrm{st,ht}} - t_{\mathrm{cs}} - \Delta T_{\mathrm{st,sp}} = \Delta T_{\mathrm{orc}} - \Delta T_{\mathrm{st,sp}} \simeq 27.5$ K (i.e. the ORC temperature drop ΔT_{orc} minus the storage spread is more or less constant). This value is likely to be a function of the isentropic efficiencies and pinches used in this model, and would deserve to be characterised for other parameters values. Note that although the heat source glide $\Delta T_{\mathrm{hs,gl}}$ has a clear increasing trend with increasing $\Delta T_{\mathrm{hs-cs}}$ (see Fig. 5), there is still a lack of convergence. This is due to the fact that this parameter does not have a direct influence on ρ_{el}, but it must have a sufficient value to ensure that the evaporation temperature in the HT-VCHP is lower than the condenser exit temperature, so as to allow significant storage temperature spreads and large large sub-cooling (see Figs. A.1i & A.1l). A beneficial consequence of this is that the exergy losses at the source are reduced. However, this heat source glide is even greater than in the case where η_{II} was maximised (i.e. it goes beyond the optimum value prescribed

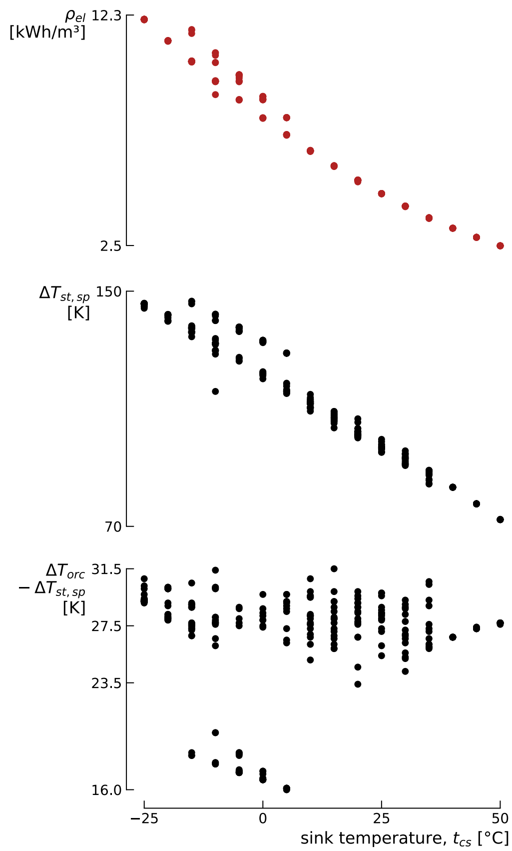

Fig. 10. Optimised energy efficiency (red dots), storage spread (black dots) and ORC temperature drop minus storage spread (black dots) depicted according to their sink temperatures.

in Section 3.1.2), which further reduces the evaporation temperature in the HT-VCHP and significantly affects COP_{hp}. As a result, η_{II} is penalised rather than favoured by this large glide.

3.2. Further design analyses

In Section 3.1, only the variables mainly affecting the *Carnot battery trilemma* have been discussed. However, parameters such as the choice of optimal fluids and the levels of super-heating and sub-cooling also play an important role. This section therefore focuses on these. In addition, it provides a graphical summary of the design guidelines obtained for TI-PTES.

3.2.1. Optimum fluids

To represent the diversity of fluids encountered over the entire domain, Fig. 11 shows a mosaic in which the colour of each tile represents one of the 34 fluids. It can be seen that

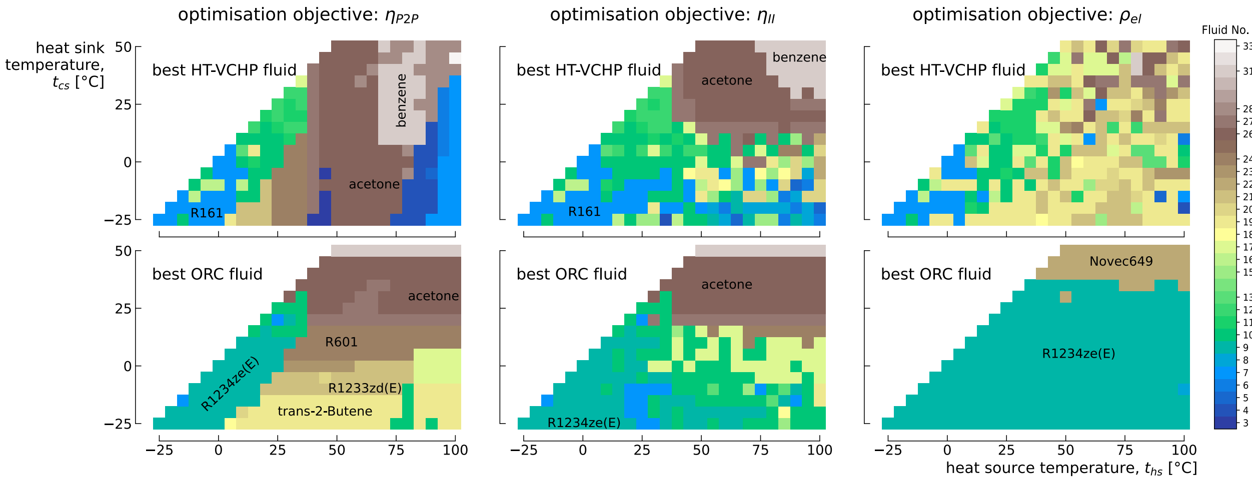

Fig. 11. Optimum fluids in the HT-VCHP (1st row) and in the ORC (2nd row) for the configurations maximising η_{P2P} (1st column), η_{II} (2nd column) and ρ_{el} (3rd column) respectively. The reason for the poor convergence for fluids maximising ρ_{el} in HT-VCHP has already been introduced in Section 3.1.3.

27 of the 34 fluids available in Table 2 are used to provide optimum performance. This illustrates well the relevance of using a method that simultaneously optimises the cycle and the choice of fluids.

Depending on the objective, the optimum fluids vary, in particular because the shape of the cycles and temperature levels change. Although there are local fluctuations, certain areas seem to be emerging. For example, in regions where the storage temperature spread $\Delta \mathrm{T}_{\mathrm{st,sp}}$ is large, *R1234ze(E)* is very often used in the ORC. It should also be noted that when η_{P2P} and η_{II} are maximised, *acetone* predominates in the HT-VCHP and in the ORC, throughout the zone where $\mathrm{t_{cs}} > 15$°C. It is also interesting to note that, at some locations, the same fluid is used in the ORC and in the HT-VCHP (e.g. *acetone*). This is an encouraging sign for the development of reversible HP/ORC systems [28, 41]. Also, when η_{P2P} is maximised, the choice of fluid in the HT-VCHP is contingent on $\mathrm{t_{hs}}$, whereas it is contingent on $\mathrm{t_{cs}}$ in the ORC. Finally, as a large number of constraints apply to the choice of fluid when designing thermal machines (e.g. maximum permitted charge, price, density, etc.), applying near optimum analyses for this phase of the design seems relevant to broaden the range of possibilities.

Although Fig. 11 is interesting for assessing the diversity of fluids encountered, it says very few about the way they are used. However, when looking at the T-s diagrams in Fig. A.1, it appears that when large $\Delta T_{st,sp}$ are used, the mode of operation in the HT-VCHP and in the ORC is usually near trans-critical. In order to map this, Fig. 12 shows the temperature difference between the critical point of the fluid and the high saturation temperature in the HT-VCHP and in the ORC. We can clearly see that in regions with large

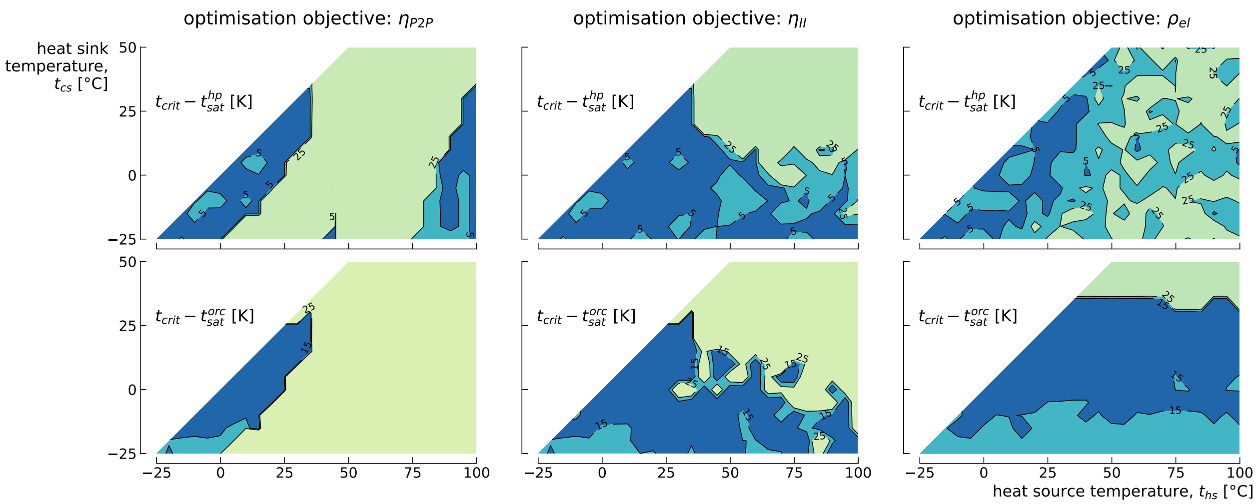

Fig. 12. Difference between critical temperature of the fluid and the high saturation temperature in the HT-VCHP (1st row) and in the ORC (2nd row). The blue zones indicates the regions where the difference is below 5 K for the HT-VCHP and below 15 K for the ORC (i.e. near trans-critical operations). In the cyan zones, this difference is below 25 K for both. It is above 25 K in the rest of the domain. The reason for the poor convergence for fluids maximising ρ_{el} in HT-VCHP has already been introduced in Section 3.1.3.

$\Delta T_{st,sp}$ (please refer to the third row of Fig. 5 to identify these zones), this temperature difference is very small. For the ORC, this can be explained by the fact that increasing the evaporation pressure (and a fortiori the evaporation temperature) reduces the calorific action required to evaporate the working fluid, and therefore maximises its efficiency. For the HT-VCHP, it can be observed that by minimising the amount of latent heat in the heat transfer with the TES, the heat exchange profile makes it possible to reduce both the exergy losses and the condensation pressure, which is favourable to the COP.

Based on these observations, it can be said that, in the regions concerned, trans-critical cycles could be good candidates for TI-PTES. Maraver *et al.* [35] have also shown that, in the case of ORC using large heat source glides, the trans-critical mode can in some cases provide efficiency gains over the sub-critical mode. However, these observations were contingent on the fluids selected and on the temperature of the heat source. Dedicated analyses would therefore be required to extend these results to TI-PTES.

3.2.2. Super-heating, sub-cooling and guidelines summary

In the HT-VCHP, the liquid sub-cooling $\Delta T_{hp,sc}$ is always maximised, so the condenser outlet temperature is equal to the cold reservoir temperature (i.e. $t_{st,ht} - \Delta T_{st,sp}$) plus the pinch ΔT_{pp}. There are therefore two pinch points, located at the condenser outlet and at the saturated vapour point. This is well illustrated in the various T-s diagrams in Fig. A.1 (although these are not strictly heat transfer diagrams). Because of its importance, this sub-cooling must be implemented and regulated using dedicated techniques. Two possible options are an active charge control in the cycle to regulate the liquid level in the condenser, or the use of a separate heat exchanger (i.e. a sub-cooler).

At the evaporator outlet, the vapour super-heating $\Delta T_{hp,sh}$ is usually maximised in order to minimise exergy losses, so the compressor supply temperature is equal to the source temperature t_{hs} minus the pinch ΔT_{pp}. Consequently, for large heat source glides and large storage spreads, this makes it possible to bring the temperature at the compressor outlet high enough to allow heat transfer with the TES thorugh de-super-heating of the vapour, while having lower condensing pressures, which increases the COP. This is clearly visible in Figs. A.1h, A.1i, A.1l in Appendix A for wet and isentropic fluids. For very dry fluids, $\Delta T_{hp,sh}$ is still maximised, although this does not allow to reduce the condensation pressure much (see Fig. A.1k).

It is interesting to note that, because of the large super-heating and de-super-heating required, these heat pump cycles are closer to the ideal Lorenz cycle (sensible heat exchange) than to the Carnot cycle (latent heat exchange). From a technological point of view, the design of the evaporator and condenser will have to be adapted to enable these cycles to be implemented, where a significant proportion of the heat exchange will be sensible, compared with the more common case where the exchange is mainly latent. This also opens up prospects for the development of new cycles, particularly those using zeotropic mixtures.

There is no strict rule for the vapour super-heating $\Delta T_{orc,sh}$ in the ORC. Based on Fig. A.1, the drier the fluid, the more $\Delta T_{orc,sh}$ will be minimised in order to limit condenser losses. In the case of isentropic fluids, $\Delta T_{orc,sh}$ will take an optimal value but not a minimum one. Finally, in the case of wet fluids (see Fig. A.1h), $\Delta T_{orc,sh}$ will have a much higher value in order to (1) ensure that the fluid is not saturated at the expander outlet and (2) minimise exergy losses at the source. This is in line with the observations reported by Maraver *et al.* [35].

At this point, it is worth making a comment on the use of recuperators in TI-PTES. In the case of the ORC, we can see that, depending on the vapour super-heating and the type of fluid used, there may be some sensible heat left at the end of expansion. This energy could be recovered through a recuperator to start economising the fluid after the pump, instead of being lost at the condenser (see Fig. A.1). However, if a very large spread is applied to the storage (= high thermal density), the temperature at the pump outlet may be very close to that of the cold tank ($t_{st,lt}$). Since this cannot be higher than $t_{st,lt} - \Delta T_{pp}$, the use of a recuperator may be problematic. It can consequently be deduced that the maximum value of the spread is constrained by the amount of heat available at the expander outlet: the higher this is, the higher the temperature of the pressurised fluid at the recuperator outlet, and therefore the more the spread is constrained. Two antagonistic mechanisms are then at work in the case of a recuperated ORC. On the one hand, the maximum thermal density is reduced, which necessarily reduces the electrical density ρ_{el}. But on the other hand, η_{orc} is increased, which increases ρ_{el}. So there is a trade-off to be found.

In the case of the HT-VCHP, it can also be seen that, depending on the liquid sub-cooling, a lot of exergy can remain at the expansion valve inlet. A simple way of recovering this exergy - without using two-phase expanders, which have low maturity levels [42, 43] - is to use a recuperator to super-heat the vapour at the compressor inlet. Here too, there are antagonist effects. On the one hand, as the vapour is hotter, the compression work is increased, which reduces $\mathrm{COP}_{\mathrm{hp}}$. But on the other hand, and in the same way as the super-heating due to the heat source glide (when any), this ensures that the vapour at the compressor outlet is sufficiently hot, which reduces the condensing pressure, which in turn reduces the work of compression and increases $\mathrm{COP}_{\mathrm{hp}}$. This logic is well illustrated by the T-s diagrams in the third column of Fig. B.1.

It is therefore clear that the use of recuperators could bring efficiency gains, but that this could affect ρ_{el}. Studies have already been carried out on this subject and have confirmed this, showing moreover that the obtained gains vary according to the objectives and to the source temperatures (the cycles maximising η_{P2P} and η_{II} do for instance not give rise to the same quantities of sensible heat and exergy to be recovered) [12]. For example, the T-s diagram in Fig. A.1d illustrates a HT-VCHP cycle where the effect of the recuperator would probably be to increase the compression work without reducing the condensing pressure, which would reduce the COP. This diagram also illustrates an ORC cycle in which there is no sensible heat to be recovered. We can therefore conclude that the recuperator is an interesting candidate for the TI-PTES, but that a case-by-case study is preferable to systematic use. This should be the subject of future work.

Finally, to graphically summarize the guidelines deduced from the maps in Section 3.1, Fig. 13 represents how to treat the main design variables according to the desired objectives in the different regions of the domain.

3.3. Multi-criteria analyses

Four locations in the domain were selected for the multi-criteria analyses. These cover the main four regions described in the maps analysis in Section 3.1 and which are depicted in the left map of Fig. 13. The corresponding Pareto fronts are shown in Fig. 14. To make

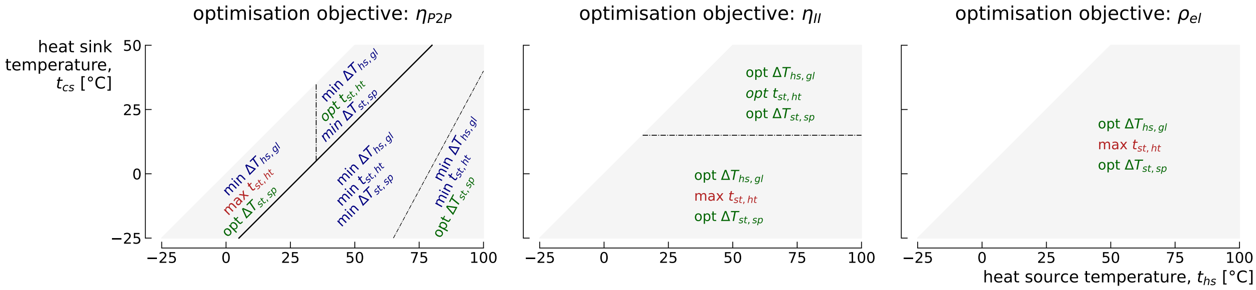

Fig. 13. Summary of the design guidelines in the different regions of the domain depending on the objectives sought. Note that only the variables have the most significant impact are reported here. "max" is for maximise and "min" for minimise. "opt" is for optimum and the corresponding optimum value is given in Section 3.1.

them easier to read, these 3D fronts are 2-dimensionalised: three fronts resulting from the conflict between each pair of objectives are represented for each location. The discontinuities observed in the various fronts are, for the most part, due to design shifts, most often caused by changes in fluid.

To quantify and map the conflict between the three objectives, the adimensionalised Euclidean distance between the best and worst performance was used:

$$\mathrm{d_{Euclidean}} = \sqrt{\left(\frac{\eta_{\mathrm{P2P}}^{\max} - \eta_{\mathrm{P2P}}^{\min}}{\eta_{\mathrm{P2P}}^{\max}}\right)^2 + \left(\frac{\eta_{\mathrm{II}}^{\max} - \eta_{\mathrm{II}}^{\min}}{\eta_{\mathrm{II}}^{\max}}\right)^2 + \left(\frac{\rho_{\mathrm{el}}^{\max} - \rho_{\mathrm{el}}^{\min}}{\rho_{\mathrm{el}}^{\max}}\right)^2} \cdot 100\ [\%] \quad . \tag{8}$$

Located in the region where $\mathrm{d_{Euclidean}} < 25\%$, the point ($\mathrm{t_{hs}} = 10$°C, $\mathrm{t_{cs}} = 10$°C) is not subject to the *trilemma*: none of the objectives is conflicting with another. Generally speaking, in that part of the domain, the best performing cycles are very similar to each other (i.e. the difference would be barely perceptible in Fig. 14) and finding an acceptable trade-off is quite straightforward.

The point ($\mathrm{t_{hs}} = 40$°C, $\mathrm{t_{cs}} = 30$°C) is located in the region where $\mathrm{t_{st,ht}}$ is not maximised when optimising η_{P2P} and η_{II}, and where $\Delta\mathrm{T_{hs,gl}}$ and $\Delta\mathrm{T_{st,sp}}$ are minimised (the difference due to their slightly different $\mathrm{t_{st,ht}}$ is not be perceptible in Fig. 14). Consequently, η_{P2P} and η_{II} do almost not conflict, but there is a slight one with ρ_{el}. This conflict is, however, of moderate intensity since maximising ρ_{el} at the expense of η_{P2P} and η_{II} only causes them to drop by 12.8% and 13.2% relatively. We can therefore conclude that maximising ρ_{el} is not

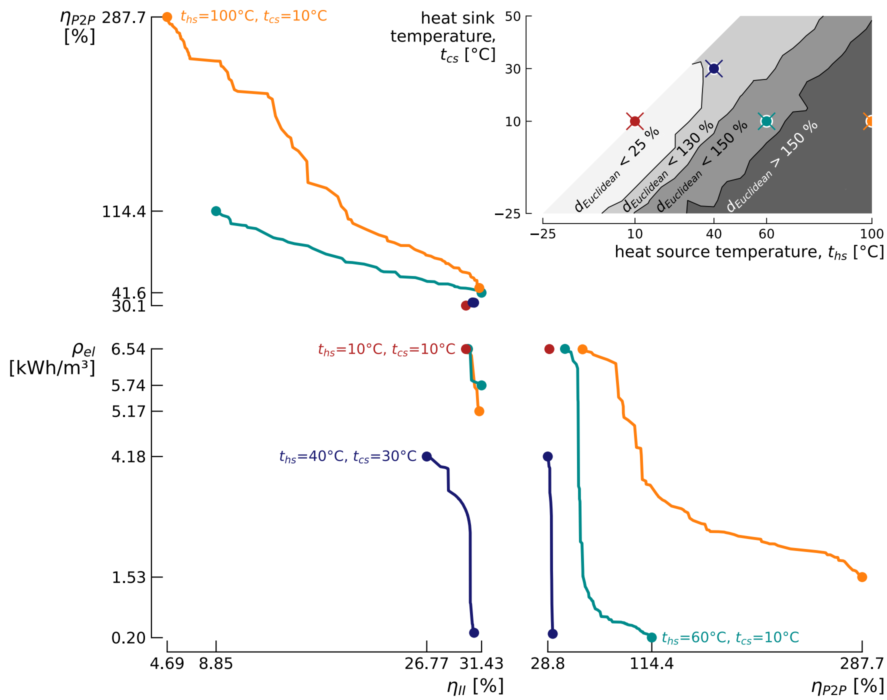

Fig. 14. Pareto fronts of the *Carnot battery trilemma* for four locations in the domain. The map of the domain shows the adimensionalised Euclidean distance between the best and worst performance of the three criteria.

too damaging to η_{P2P} and η_{II}, and that the *trilemma* is weak at this point. This illustrates once again that different designs can give very similar performance and that conducting near optimum analysis would be relevant for the study of TI-PTES.

In contrast, Fig. 14 shows that the *trilemma* is much more intense for the point ($\mathrm{t_{hs}}$ = 60°C, $\mathrm{t_{cs}}$ = 10°C). The front between η_{P2P} and η_{II} is linear, and it results mainly of a simultaneous trade-off between $\Delta\mathrm{T_{hs,gl}}$, $\mathrm{t_{st,ht}}$ and $\Delta\mathrm{T_{st,sp}}$, which in line with the observations drawn Section 3.1. The steep front between ρ_{el} and η_{P2P} illustrates well the very binary nature of the problem: it is not really possible to obtain a satisfactory trade-off between the two criteria, as one tends to clearly degrade the other. Indeed, the maximisation of η_{P2P} requires minimising $\Delta\mathrm{T_{hs,gl}}$, $\mathrm{t_{st,ht}}$ and $\Delta\mathrm{T_{st,sp}}$ whereas opposite trends are observed for ρ_{el}. However, we note that for the point ($\mathrm{t_{hs}}$ = 100°C, $\mathrm{t_{cs}}$ = 10°C), which lies in the area where $\Delta\mathrm{T_{st,sp}}$ is slightly increased to maximise η_{P2P}, the minimum density is thereby increased, which has the effect of slightly reducing the *trilemma*.

When designing a Carnot battery in this part of the domain, one approach to arbitrating the *trilemma* and identifying optimal storage temperatures is to introduce the economic dimension. For known cost functions of each of the Carnot battery's components, the aim of optimising the thermodynamic design will be to optimise an economic criterion, such as the Levelised Cost Of Storage (which is actually a function of η_{P2P}, η_{II} and ρ_{el}). It should be stressed, however, that identifying such cost functions is not trivial, as they are non-constant and generally non-linear (e.g. the higher the storage temperature, the more expensive it will be).

Finally, it can be noted that, in the region where $\mathrm{d}_{\mathrm{Euclidean}} > 150\%$, ρ_{el} and η_{II} are much less conflicting with each other than with η_{P2P}. This is largely due to the fact that they both maximise the storage temperature and that they need a large storage spread. They also both require large heat source glides, in one case to ensure an effective waste heat recovery (i.e. maximisation of η_{II}) and in a second case to allow large spreads (i.e. maximisation of ρ_{el} and η_{II}). All in all, this result tends to prove that the trilemma is essentially caused by the maximisation of η_{P2P} - which moreover leads to a TI-PTES degenerated into a TES + ORC, which no longer makes it a genuine electricity storage system but rather a pure waste heat recovery system (see Section 3.1.1).

4. Conclusion and perspectives

This work looked at the *Carnot battery trilemma* for sub-critical cycles over an extended thermal integration domain. Using an in-house thermodynamic model and thanks to a genetic algorithm, multi-criteria optimisation was used to map the maximum theoretical performance that could be provided by TI-PTES in terms of power-to-power efficiency η_{P2P} (i.e. quality of electricity recovery), exergy efficiency η_{II} (i.e. quality of combined heat and electricity recovery) and electrical energy density ρ_{el} (i.e. storage size). Eight optimization variables were used, including both the parameters of the thermodynamic cycles and the choice of working fluids. The multi-criteria analysis also made it possible to characterise the nature of the conflict between these objectives, in particular by analysing the shape of the Pareto fronts obtained. The main conclusions of this work are:

- When optimised, η_{P2P} grows with the temperature difference between the source and sink $\Delta\mathrm{T}_{\mathrm{hs-cs}}$. This growth is however not continuous because of a design shift. For $\Delta\mathrm{T}_{\mathrm{hs-cs}} \leq 30$ K, the storage temperature $\mathrm{t}_{\mathrm{st,ht}}$ is maximised, whereas it is minimised for $\Delta\mathrm{T}_{\mathrm{hs-cs}} > 30$ K. For its part, η_{II} decreases as the sink temperature t_{cs} increases, because the ORC efficiency η_{orc} falls. However, for $\mathrm{t}_{\mathrm{cs}} > 15$°C, η_{orc} (and therefore η_{II}) stabilises thanks to a design shift ($\mathrm{t}_{\mathrm{st,ht}}$ and the storage spread $\Delta\mathrm{T}_{\mathrm{st,sp}}$ are reduced). Finally, ρ_{el} decreases as t_{cs} increases, both because the thermal density and η_{orc} decrease.

- Guidelines for maximising each of the *trilemma* objectives have been formulated over the entire thermal domain. However, these are not uniform across the domain and are adapted in the different sub-regions. Some of these sub-regions are linked to the thermodynamics of TI-PTES (e.g. choice of the optimal $\mathrm{t}_{\mathrm{st,ht}}$ as a function of heat transfer irreversibilities) while others are linked to the technological constraints imposed (e.g. choice of the optimal $\mathrm{t}_{\mathrm{st,ht}}$ as a function of the maximum $\mathrm{t}_{\mathrm{st,ht}}$ allowed). This result highlights the importance of considering these constraints when formulating design guidelines, since optimal cycles obtained can deviate from theory.

- There is a strong synergy between $\mathrm{t}_{\mathrm{st,ht}}$ and $\Delta\mathrm{T}_{\mathrm{st,sp}}$, which are two main design variables in TI-PTES with sensible heat storage. When $\mathrm{t}_{\mathrm{st,ht}}$ is high, which is in favour of η_{orc} but penalises $\mathrm{COP}_{\mathrm{hp}}$, $\Delta\mathrm{T}_{\mathrm{st,sp}}$ is also large so as to maintain a sufficiently high $\mathrm{COP}_{\mathrm{hp}}$, which in fact also reduces η_{orc}. The conflict between $\mathrm{COP}_{\mathrm{hp}}$ and η_{orc} is therefore resolved by simultaneously adjusting $\mathrm{t}_{\mathrm{st,ht}}$ and $\Delta\mathrm{T}_{\mathrm{st,sp}}$. Maximising $\mathrm{COP}_{\mathrm{hp}}$ using larger spreads is achieved by lowering the condensation pressure in the HT-VCHP and by maximising the sub-cooling. Conversely, when $\mathrm{t}_{\mathrm{st,ht}}$ is minimised (i.e. the heat pump lift is minimised), $\Delta\mathrm{T}_{\mathrm{st,sp}}$ is also generally minimised, so as to approach ideal Carnot cycles.

- The intensity of the *trilemma*, which is measured by the Euclidean distance between the maximum and minimum values of the objectives, increases as ΔT_{hs-cs} increases. This suggests that the *trilemma* is driven by η_{P2P}, while the conflict between η_{II} and ρ_{el} is much weaker. The hinge variable is $t_{st,ht}$, which is minimised for η_{P2P} when $\Delta T_{hs-cs} > 30$ K, and is maximised in the other cases. Below this tipping point (i.e. $\Delta T_{hs-cs} \leq 30$ K), the intensity of the *trilemma* is therefore lower.

- Overall, the concept of thermal integration for PTES should be reconsidered. While it was introduced in 2017 to artificially increase η_{P2P}, we can see that, for $\Delta T_{hs-cs} > 30$ K, maximising this parameter leads to very low η_{II} and ρ_{el}. Moreover, the TI-PTES degenerates into a TES + ORC (i.e. zero contribution from the heat pump), which makes it a heat recovery option but no longer an electrical storage system as such. However, the majority of studies to date have focused on $\Delta T_{hs-cs} > 45$ K, because η_{P2P} is much better there. Yet, a nuance needs to be introduced: in cases where the heat source glide is constrained (e.g. frequently at 10 K in cooling applications), the exergy losses from the source to the environment disappear, which relatively increases η_{II}. Still, maximising η_{P2P} will always lead to minimising $t_{st,ht}$, which will penalise ρ_{el} and still lead to a degenerated TI-PTES. So, to recover waste heat when $\Delta T_{hs-cs} > 30$ K, there are probably solutions that are more exergy- and financially-effective than TI-PTES.

On the basis of the results obtained, prospects for future work can also be given:

- In view of the large spreads involved and the fact that the critical points of the selected fluids are generally well below $t_{st,ht}$, the study of trans-critical cycles in TI-PTES applications seems to be of interest. A second avenue worth investigating is zeotropic mixtures. Future work could characterise and optimise these systems to see if they can reduce the *Carnot battery trilemma* and increase the performance.

- Systematic consideration of the use of a recuperator in the HT-VCHP and in the ORC also seems essential. However, as discussed, this will not systematically result in better performance and must therefore be assessed on a case-by-case basis.

- This thermodynamic study showed that taking into account technological constraints (e.g. maximum $t_{st,ht}$, maximum cycles temperature, minimum pressure) caused deviations between the theory and the actually optimal cycles. Taking greater account of these technological constraints (e.g. maximum compression ratio, etc.) would therefore be appropriate in future work.

- Finally, the application of near-optimum analyses to the study of TI-PTES could potentially make new designs emerge. In particular, tolerating (very) slight performance degradation could make it possible to find configurations that are, for instance, less prone to the *trilemma*, or cheaper to implement (e.g. lower storage temperature). This would also make it possible to identify designs that are less sensitive to slight deviations of parameters from nominal conditions, which is very useful in operational analyses (e.g. degree of super-heating, of sub-cooling, pinches, etc.). Eventually, this would enable to characterise which parameters should not deviate from nominal conditions, which would enable effective control strategies.

Declaration of competing interest

The authors declare that they have no known competing financial interests or personal relationships that could have appeared to influence the work reported in this paper.

Acknowledgements

The first author acknowledges the support of Fonds de la Recherche Scientifique - FNRS [40014566 FRIA-B1].

Computational resources have been provided by the Consortium des Équipements de Calcul Intensif (CÉCI), funded by the Fonds de la Recherche Scientifique de Belgique (F.R.S.-FNRS) under Grant No. 2.5020.11 and by the Walloon Region.

Appendix A. Representative T-s diagrams

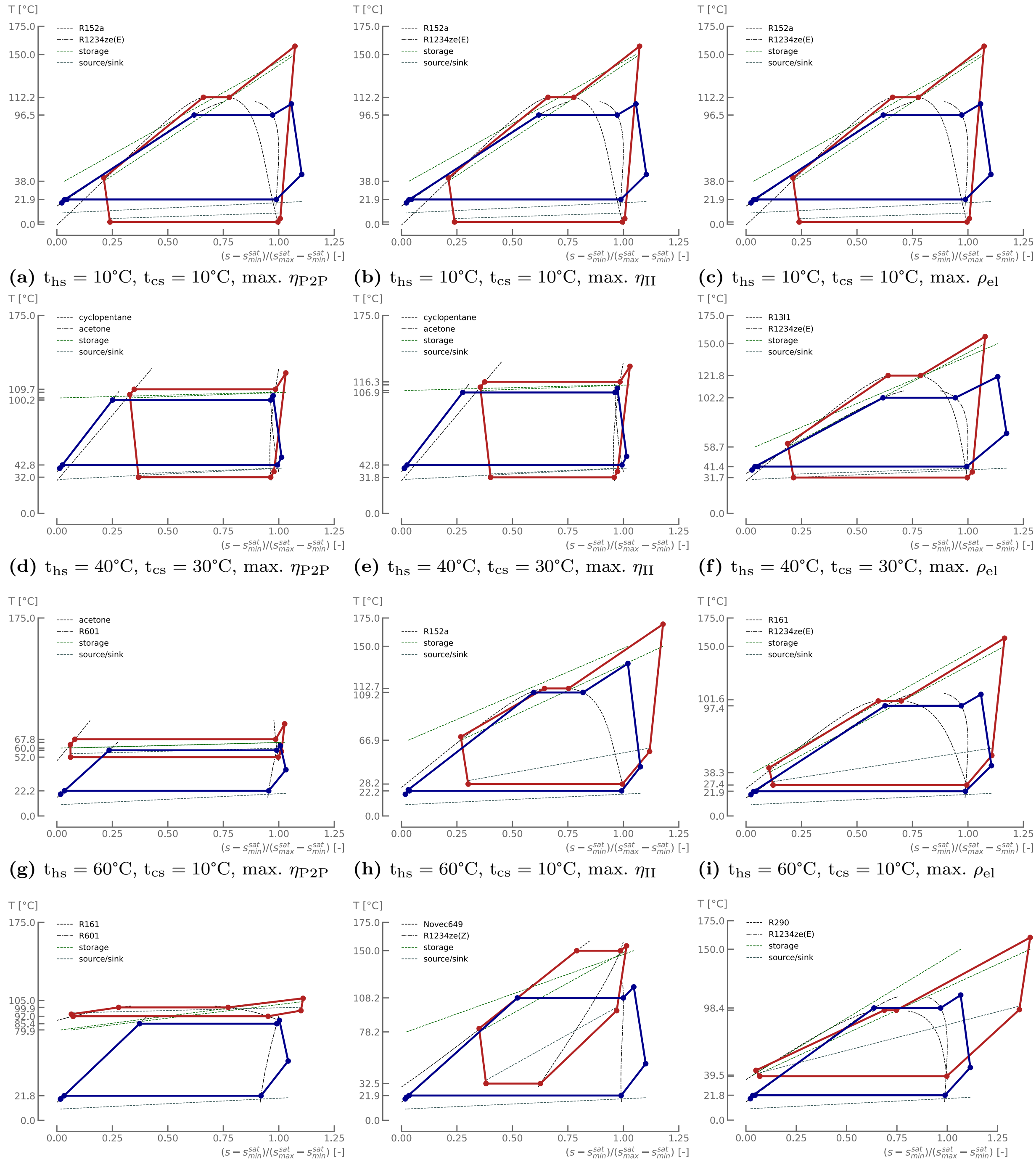

(a) $t_{hs} = 10°C$, $t_{cs} = 10°C$, max. η_{P2P} **(b)** $t_{hs} = 10°C$, $t_{cs} = 10°C$, max. η_{II} **(c)** $t_{hs} = 10°C$, $t_{cs} = 10°C$, max. ρ_{el}

(d) $t_{hs} = 40°C$, $t_{cs} = 30°C$, max. η_{P2P} **(e)** $t_{hs} = 40°C$, $t_{cs} = 30°C$, max. η_{II} **(f)** $t_{hs} = 40°C$, $t_{cs} = 30°C$, max. ρ_{el}

(g) $t_{hs} = 60°C$, $t_{cs} = 10°C$, max. η_{P2P} **(h)** $t_{hs} = 60°C$, $t_{cs} = 10°C$, max. η_{II} **(i)** $t_{hs} = 60°C$, $t_{cs} = 10°C$, max. ρ_{el}

(j) $t_{hs} = 100°C$, $t_{cs} = 10°C$, max. η_{P2P} **(k)** $t_{hs} = 100°C$, $t_{cs} = 10°C$, max. η_{II} **(l)** $t_{hs} = 100°C$, $t_{cs} = 10°C$, max. ρ_{el}

Fig. A.1. T-s diagrams of the configurations maximising η_{P2P}, η_{II} and ρ_{el} for four different locations in the domain. Red solid lines are for the HT-VCHP and the blue ones are for the ORC. Green dashed lines correspond to the TES and are placed to illustrate the heat transfer with the cycles, though these are not proper representations for pinch analyses. Grey dashed lines represent the source and the sink.

Appendix B. Synergies between technological constraints and optimum cycles

The analysis carried out in Section 3.1.1 showed that, for endoreversible cycles (i.e. no internal irreversibilities) but considering irreversibilities at the heat transfers with the source, the thermal storage and the sink, there is a threshold in terms of temperature difference between the source and the sink below (resp. above) which the storage temperature must be maximised (resp. minimised) in order to maximise the power-to-power efficiency η_{P2P} of TI-PTES. It was also demonstrated that this threshold is a function of the irreversibilities at the heat transfers. This result is reflected in the fact that below the threshold, the ORC efficiency is favoured, whereas above the threshold, the COP of the HT-VCHP is favoured.

The optimisation results are consistent with this simplified theoretical analysis. However, it can be observed that, below the threshold (i.e. $\Delta \mathrm{T}_{\mathrm{hs-cs}} \leq 30$ K) and for superior sink temperatures (i.e. $\mathrm{t}_{\mathrm{cs}} > 15$°C), the storage temperature is no longer maximised but takes on an optimum value, meaning that, in that part of the domain, there is an optimum trade-off to find between the COP of the HT-VCHP and the ORC efficiency. This observation can also be extrapolated to the case of maximising the exergy efficiency where, for any source temperature and for sink temperatures above 15°C, the storage temperature takes on an optimum value rather than being maximised.

At least two hypotheses can be put forward to explain this observation. The first is linked to the constraint on the maximum cycle and storage temperatures. The second is linked to the constraint on the available fluids and the minimum pressure in the heat exchangers. As shown below, the second can easily be ruled out, which leads to the conclusion that it is indeed the constraint on the maximum temperatures that causes this deviation of the optimum storage temperature from theory.

Appendix B.1. Maximum temperature constraint

When η_{P2P} is maximised, because of the constraint $\mathrm{t}_{\mathrm{st,ht}}^{\mathrm{max}} = 150$°C, the ORC efficiency decreases as the sink temperature increases (the temperature difference between its source and its sink decreases). Above a certain threshold (around 15°C in the present case), this efficiency becomes so low that $\mathrm{COP}_{\mathrm{hp}}$ must be increased in order to maintain η_{P2P} at

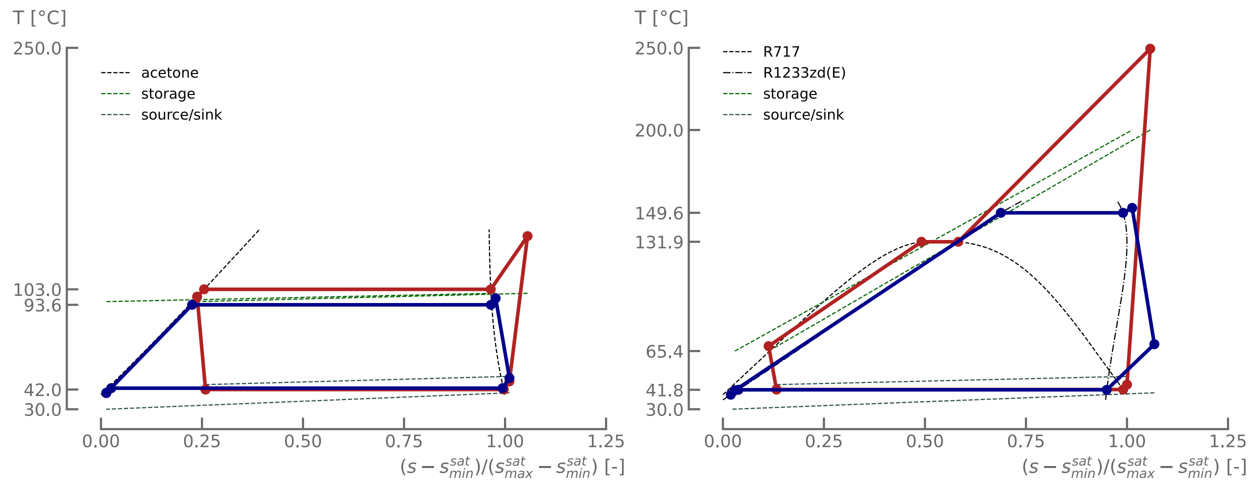

(a) Original constraints: $\mathrm{t_{st,ht}^{max}} = 150$°C and $\mathrm{t_{hp}^{max}} = 180$°C **(b)** Relaxed constraints: $\mathrm{t_{st,ht}^{max}} = 200$°C and $\mathrm{t_{hp}^{max}} = 300$°C

Fig. B.1. T-s diagrams of the configurations maximising η_{P2P} for $\mathrm{t_{hs}} = 50$°C and $\mathrm{t_{cs}} = 30$°C with the original (left) and relaxed (right) constraints. Red solid lines are for the HT-VCHP and the blue ones are for the ORC. Green dashed lines correspond to the TES and are placed to illustrate the heat transfer with the cycles, though these are not proper representations for pinch analyses. Grey dashed lines represent the source and the sink. The corresponding efficiencies are $\eta_{\mathrm{P2P}}^{\mathrm{original}} = 39.7\%$ and $\eta_{\mathrm{P2P}}^{\mathrm{relaxed}} = 43.0\%$.

maximum values. As a result, the storage temperature has to be lowered, which further affects the ORC efficiency. There is therefore an optimum trade-off to find between η_{orc} and $\mathrm{COP_{hp}}$.

In order to verify this hypothesis, the $\mathrm{t_{st,ht}^{max}} = 150$°C constraint was increased to $\mathrm{t_{st,ht}^{max}} = 200$°C in a cell of domain located in the region concerned ($\mathrm{t_{hs}} = 50$°C, $\mathrm{t_{cs}} = 30$°C). The maximum temperature in the HT-VCHP was also raised to $\mathrm{t_{hp}^{max}} = 300$°C instead of $\mathrm{t_{hp}^{max}} = 180$°C to enable $\mathrm{t_{st,ht}^{max}}$ to be reached during the optimisation (although this is probably beyond the current technological limits for HT-VCHP). The storage pressure was set to 20 bar. The optimisation was then restarted. Fig. B.1 depicts the T-s diagrams of the TI-PTES cycles maximising η_{P2P} with the original (Fig. B.1a) and relaxed (Fig. B.1b) constraints. It can be seen from Fig. B.1 that, as expected, the $\mathrm{t_{st,ht}^{max}} = 200$°C constraint gives rise to a design that maximises the storage temperature (i.e. $\mathrm{t_{st,ht}} = 200$°C) in order to maximise η_{P2P}. As a result, the latter gains more than three points by going from 39.7% to 43.0%.

To the best of the authors' knowledge, this observation on the optimum storage temperature has not yet been made in the literature. It would therefore be appropriate for this observation to be confirmed by further studies. In addition, it would be interesting to carry out sensitivity analyses and apply near-optimum analyses in order to assess the extent to which η_{P2P} (and η_{II}) would be affected by maximising the storage temperature when the constraint $\mathrm{t}_{\mathrm{st,ht}}^{\mathrm{max}} = 150$°C is maintained.

Appendix B.2. Minimum pressure constraint

Another explanation for why the storage temperature is not maximised when the sink is above 15°C could be the unavailability of fluids in that temperature range, due to the constraint $\mathrm{p}_{\mathrm{min}} = 0.5$ bar. Indeed, the higher the critical temperature, the lower the saturation pressure at a given temperature (see Fig. B.2). It could therefore be envisaged that no fluid respects constraint $\mathrm{p}_{\mathrm{min}} = 0.5$ bar when the storage temperature is 150°C, because higher critical temperatures are needed to operate the cycle in sub-critical regime. However, this hypothesis can be dismissed out of hand. First, because there are fluids that allow $\mathrm{t}_{\mathrm{st,ht}} = 150$°C in the $\mathrm{t}_{\mathrm{cs}} \leq 15$°C zone, which is actually even more constrained than the zone where $\mathrm{t}_{\mathrm{cs}} > 15$°C (see Fig. 5). Second, because Fig. B.2 shows that there are fluids with a critical point above 150°C which meet the constraint.

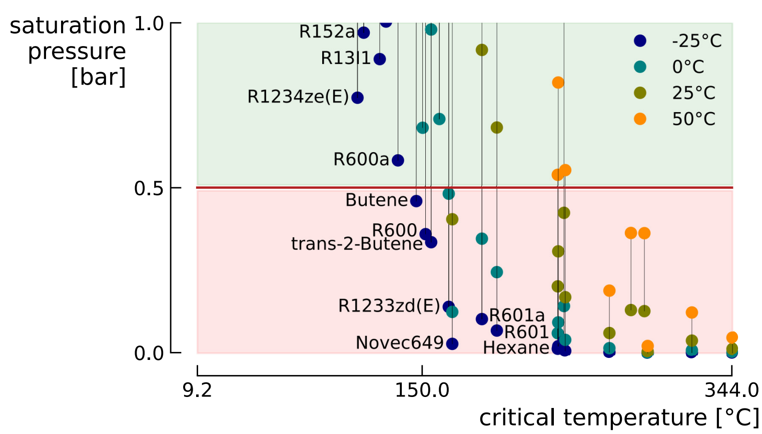

Fig. B.2. Saturation pressure at four different temperatures for the 34 fluids considered in this study. It can be seen that those with a higher critical temperature tend to have lower saturation pressures, which can be detrimental to compliance with the constraint $\mathrm{p}_{\mathrm{hp/orc}}^{\mathrm{min}} \geq 0.5$ bar.

References

[1] Buildings, in: Intergovernmental Panel on Climate Change (IPCC) (Ed.), Climate Change 2022 - Mitigation of Climate Change, 1st Edition, Cambridge University Press, 2023, pp. 953–1048. doi:10.1017/9781009157926.011.
URL https://www.cambridge.org/core/product/identifier/9781009157926%23c9/type/book_part

[2] C. Forman, I. K. Muritala, R. Pardemann, B. Meyer, Estimating the global waste heat potential, Renewable and Sustainable Energy Reviews 57 (2016) 1568–1579. doi:10.1016/j.rser.2015.12.192.
URL https://www.sciencedirect.com/science/article/pii/S1364032115015750

[3] S. Koohi-Fayegh, M. A. Rosen, A review of energy storage types, applications and recent developments, Journal of Energy Storage 27 (2020) 101047. doi:10.1016/j.est.2019.101047.
URL https://www.sciencedirect.com/science/article/pii/S2352152X19306012

[4] H. Jockenhöfer, W.-D. Steinmann, D. Bauer, Detailed numerical investigation of a pumped thermal energy storage with low temperature heat integration, Energy 145 (2018) 665–676. doi:10.1016/j.energy.2017.12.087.
URL https://linkinghub.elsevier.com/retrieve/pii/S0360544217321308

[5] M. Astolfi, R. Aumann, M. Baresi, D. Batscha, J. van Buijten, F. Casella, P. Colonna, G. David, S. Karellas, W. Klink, A. Fiterman, G. Mariotti, H. Ohman, L. Ribarov, M. Ruggiero, D. Sanchez, C. Wieland, G. Zamperi, Thermal Energy Harvesting - the Path to Tapping into a Large CO2-free European Power Source, Tech. Rep. Version 1.0, Knowledge Center on Organic Rankine Cycle technology (Apr. 2022).
URL https://kcorc.org/en/committees/thermal-energy-harvesting-advocacy-group/

[6] A. Marina, S. Spoelstra, H. A. Zondag, A. K. Wemmers, An estimation of the European industrial heat pump market potential, Renewable and Sustainable Energy Reviews 139

(2021) 110545. doi:10.1016/j.rser.2020.110545.
URL https://www.sciencedirect.com/science/article/pii/S1364032120308297

[7] S. Lecompte, H. Huisseune, M. van den Broek, B. Vanslambrouck, M. De Paepe, Review of organic Rankine cycle (ORC) architectures for waste heat recovery, Renewable and Sustainable Energy Reviews 47 (2015) 448–461. doi:10.1016/j.rser.2015.03.089.
URL https://www.sciencedirect.com/science/article/pii/S1364032115002427

[8] S. Quoilin, S. Declaye, B. F. Tchanche, V. Lemort, Thermo-economic optimization of waste heat recovery Organic Rankine Cycles, Applied Thermal Engineering 31 (14) (2011) 2885–2893. doi:10.1016/j.applthermaleng.2011.05.014.
URL https://www.sciencedirect.com/science/article/pii/S1359431111002663

[9] G. F. Frate, M. Antonelli, U. Desideri, A novel Pumped Thermal Electricity Storage (PTES) system with thermal integration, Applied Thermal Engineering 121 (2017) 1051–1058. doi:10.1016/j.applthermaleng.2017.04.127.
URL https://linkinghub.elsevier.com/retrieve/pii/S135943111634114X

[10] M. Mercangöz, J. Hemrle, L. Kaufmann, A. Z'Graggen, C. Ohler, Electrothermal energy storage with transcritical CO2 cycles, Energy 45 (1) (2012) 407–415. doi:10.1016/j.energy.2012.03.013.
URL https://linkinghub.elsevier.com/retrieve/pii/S0360544212002046

[11] W. D. Steinmann, The CHEST (Compressed Heat Energy STorage) concept for facility scale thermo mechanical energy storage, Energy 69 (2014) 543–552. doi:10.1016/j.energy.2014.03.049.
URL http://www.sciencedirect.com/science/article/pii/S0360544214003132

[12] G. F. Frate, L. Ferrari, U. Desideri, Multi-criteria investigation of a pumped thermal electricity storage (PTES) system with thermal integration and sensible heat storage, Energy Conversion and Management 208 (2020) 112530. doi:

10.1016/j.enconman.2020.112530.
URL https://linkinghub.elsevier.com/retrieve/pii/S0196890420300662

[13] M. Weitzer, D. Müller, J. Karl, Two-phase expansion processes in heat pump – ORC systems (Carnot batteries) with volumetric machines for enhanced off-design efficiency, Renewable Energy 199 (2022) 720–732. doi:10.1016/j.renene.2022.08.143.
URL https://www.sciencedirect.com/science/article/pii/S0960148122013222

[14] G. F. Frate, L. Ferrari, U. Desideri, Multi-Criteria Economic Analysis of a Pumped Thermal Electricity Storage (PTES) With Thermal Integration, Frontiers in Energy Research 8 (2020) 53. doi:10.3389/fenrg.2020.00053.
URL https://www.frontiersin.org/article/10.3389/fenrg.2020.00053/full

[15] M. Weitzer, D. Müller, D. Steger, A. Charalampidis, S. Karellas, J. Karl, Organic flash cycles in Rankine-based Carnot batteries with large storage temperature spreads, Energy Conversion and Management 255 (2022) 115323. doi:10.1016/j.enconman.2022.115323.
URL https://www.sciencedirect.com/science/article/pii/S0196890422001194

[16] P. Lu, X. Luo, J. Wang, J. Chen, Y. Liang, Z. Yang, J. He, C. Wang, Y. Chen, Thermodynamic analysis and evaluation of a novel composition adjustable Carnot battery under variable operating scenarios, Energy Conversion and Management 269 (2022) 116117. doi:10.1016/j.enconman.2022.116117.
URL https://www.sciencedirect.com/science/article/pii/S0196890422009013

[17] M. Zhang, L. Shi, P. Hu, G. Pei, G. Shu, Carnot battery system integrated with low-grade waste heat recovery: Toward high energy storage efficiency, Journal of Energy Storage 57 (2023) 106234. doi:10.1016/j.est.2022.106234.
URL https://www.sciencedirect.com/science/article/pii/S2352152X2202223X

[18] E. Bellos, Thermodynamic analysis of a Carnot battery unit with double exploitation of a waste heat source, Energy Conversion and Management 299 (2024) 117844. doi:

10.1016/j.enconman.2023.117844.
URL https://www.sciencedirect.com/science/article/pii/S0196890423011901

[19] O. Dumont, V. Lemort, Mapping of performance of pumped thermal energy storage (Carnot battery) using waste heat recovery, Energy 211 (2020) 118963. doi:10.1016/j.energy.2020.118963.
URL https://linkinghub.elsevier.com/retrieve/pii/S0360544220320703

[20] R. Xia, Z. Wang, M. Cao, Y. Jiang, H. Tang, Y. Ji, F. Han, Comprehensive performance analysis of cold storage Rankine Carnot batteries: Energy, exergy, economic, and environmental perspectives, Energy Conversion and Management 293 (2023) 117485. doi:10.1016/j.enconman.2023.117485.
URL https://www.sciencedirect.com/science/article/pii/S0196890423008312

[21] S. Hu, Z. Yang, J. Li, Y. Duan, Thermo-economic analysis of the pumped thermal energy storage with thermal integration in different application scenarios, Energy Conversion and Management 236 (2021) 114072. doi:10.1016/j.enconman.2021.114072.
URL https://linkinghub.elsevier.com/retrieve/pii/S019689042100248X

[22] R. Fan, H. Xi, Energy, exergy, economic (3E) analysis, optimization and comparison of different Carnot battery systems for energy storage, Energy Conversion and Management 252 (2022) 115037. doi:10.1016/j.enconman.2021.115037.
URL https://www.sciencedirect.com/science/article/pii/S0196890421012139

[23] Y. Zhang, L. Xu, J. Li, L. Zhang, Z. Yuan, Technical and economic evaluation, comparison and optimization of a Carnot battery with two different layouts, Journal of Energy Storage 55 (2022) 105583. doi:10.1016/j.est.2022.105583.
URL https://www.sciencedirect.com/science/article/pii/S2352152X22015717

[24] X. Yu, H. Qiao, B. Yang, H. Zhang, Thermal-economic and sensitivity analysis of different Rankine-based Carnot battery configurations for energy storage, Energy Conversion

and Management 283 (2023) 116959. doi:10.1016/j.enconman.2023.116959.
URL https://www.sciencedirect.com/science/article/pii/S0196890423003059

[25] X. Zhang, Y. Sun, W. Zhao, C. Li, C. Xu, H. Sun, Q. Yang, X. Tian, D. Wang, The Carnot batteries thermally assisted by the steam extracted from thermal power plants: A thermodynamic analysis and performance evaluation, Energy Conversion and Management 297 (2023) 117724. doi:10.1016/j.enconman.2023.117724.
URL https://www.sciencedirect.com/science/article/pii/S0196890423010701

[26] H. Qiao, X. Yu, B. Yang, Working fluid design and performance optimization for the heat pump-organic Rankine cycle Carnot battery system based on the group contribution method, Energy Conversion and Management 293 (2023) 117459. doi:10.1016/j.enconman.2023.117459.
URL https://www.sciencedirect.com/science/article/pii/S0196890423008051

[27] Z. Wang, R. Xia, Y. Jiang, M. Cao, Y. Ji, F. Han, Evaluation and optimization of an engine waste heat assisted Carnot battery system for ocean-going vessels during harbor stays, Journal of Energy Storage 73 (2023) 108866. doi:10.1016/j.est.2023.108866.
URL https://www.sciencedirect.com/science/article/pii/S2352152X23022636

[28] S. Staub, P. Bazan, K. Braimakis, D. Müller, C. Regensburger, D. Scharrer, B. Schmitt, D. Steger, R. German, S. Karellas, M. Pruckner, E. Schlücker, S. Will, J. Karl, Reversible Heat Pump–Organic Rankine Cycle Systems for the Storage of Renewable Electricity, Energies 11 (6) (2018) 1352, number: 6 Publisher: Multidisciplinary Digital Publishing Institute. doi:10.3390/en11061352.
URL https://www.mdpi.com/1996-1073/11/6/1352

[29] K. S. Reddy, V. Mudgal, T. K. Mallick, Review of latent heat thermal energy storage for improved material stability and effective load management, Journal of Energy Storage 15 (2018) 205–227. doi:10.1016/j.est.2017.11.005.
URL https://www.sciencedirect.com/science/article/pii/S2352152X1730227X

[30] I. H. Bell, J. Wronski, S. Quoilin, V. Lemort, Pure and pseudo-pure fluid thermophysical property evaluation and the open-source thermophysical property library CoolProp, Industrial & engineering chemistry research 53 (6) (2014) 2498–2508, publisher: ACS Publications.

[31] G. F. Frate, L. Ferrari, U. Desideri, Analysis of suitability ranges of high temperature heat pump working fluids, Applied Thermal Engineering 150 (2019) 628–640. doi:10.1016/j.applthermaleng.2019.01.034.
URL https://www.sciencedirect.com/science/article/pii/S1359431118353602

[32] C. Arpagaus, F. Bless, M. Uhlmann, J. Schiffmann, S. S. Bertsch, High temperature heat pumps: Market overview, state of the art, research status, refrigerants, and application potentials, Energy 152 (2018) 985–1010. doi:10.1016/j.energy.2018.03.166.
URL https://www.sciencedirect.com/science/article/pii/S0360544218305759

[33] T. Ommen, J. K. Jensen, W. B. Markussen, L. Reinholdt, B. Elmegaard, Technical and economic working domains of industrial heat pumps: Part 1 – Single stage vapour compression heat pumps, International Journal of Refrigeration 55 (2015) 168–182. doi:10.1016/j.ijrefrig.2015.02.012.
URL https://www.sciencedirect.com/science/article/pii/S0140700715000444

[34] J. Jiang, B. Hu, R. Z. Wang, N. Deng, F. Cao, C.-C. Wang, A review and perspective on industry high-temperature heat pumps, Renewable and Sustainable Energy Reviews 161 (2022) 112106. doi:10.1016/j.rser.2022.112106.
URL https://www.sciencedirect.com/science/article/pii/S1364032122000351

[35] D. Maraver, J. Royo, V. Lemort, S. Quoilin, Systematic optimization of subcritical and transcritical organic Rankine cycles (ORCs) constrained by technical parameters in multiple applications, Applied Energy 117 (2014) 11–29. doi:10.1016/j.apenergy.2013.11.076.
URL https://www.sciencedirect.com/science/article/pii/S0306261913009859

[36] C. Smith, Z. Nicholls, K. Armour, W. Collins, P. Forster, M. Meinshausen, M. Palmer, M. Watanabe, The Earth's Energy Budget, Climate Feedbacks, and Climate Sensitivity Supplementary Material, in: V. Masson-Delmotte, P. Zhai, A. Pirani, S. Connors, C. Péan, S. Berger, N. Caud, Y. Chen, L. Goldfarb, M. Gomis, M. Huang, K. Leitzell, E. Lonnoy, J. Matthews, T. Maycock, T. Waterfield, O. Yelekçi, R. Yu, B. Zhou (Eds.), Climate Change 2021: The Physical Science Basis. Contribution of Working Group I to the Sixth Assessment Report of the Intergovernmental Panel on Climate Change, 2021, type: Book Section.
URL `Availablefromhttps://www.ipcc.ch/`

[37] K. Deb, A. Pratap, S. Agarwal, T. Meyarivan, A fast and elitist multiobjective genetic algorithm: NSGA-II, IEEE transactions on evolutionary computation 6 (2) (2002) 182–197, publisher: IEEE.

[38] D. Coppitters, P. Tsirikoglou, W. D. Paepe, K. Kyprianidis, A. Kalfas, F. Contino, RHEIA: Robust design optimization of renewable Hydrogen and dErIved energy cArrier systems, Journal of Open Source Software 7 (75) (2022) 4370. `doi:10.21105/joss.04370`.
URL `https://joss.theoj.org/papers/10.21105/joss.04370`

[39] J. Blank, K. Deb, Pymoo: Multi-Objective Optimization in Python, IEEE Access 8 (2020) 89497–89509, conference Name: IEEE Access. `doi:10.1109/ACCESS.2020.2990567`.
URL `https://ieeexplore.ieee.org/document/9078759`

[40] P. Voll, M. Jennings, M. Hennen, N. Shah, A. Bardow, The optimum is not enough: A near-optimal solution paradigm for energy systems synthesis, Energy 82 (2015) 446–456. `doi:10.1016/j.energy.2015.01.055`.
URL `https://www.sciencedirect.com/science/article/pii/S0360544215000791`

[41] O. Dumont, S. Quoilin, V. Lemort, Experimental investigation of a reversible heat pump/organic Rankine cycle unit designed to be coupled with a passive house to get

a Net Zero Energy Building, International Journal of Refrigeration 54 (2015) 190–203. doi:10.1016/j.ijrefrig.2015.03.008.
URL https://linkinghub.elsevier.com/retrieve/pii/S0140700715000638

[42] A. A. Murthy, A. Subiantoro, S. Norris, M. Fukuta, A review on expanders and their performance in vapour compression refrigeration systems, International Journal of Refrigeration 106 (2019) 427–446. doi:10.1016/j.ijrefrig.2019.06.019.
URL https://www.sciencedirect.com/science/article/pii/S0140700719302701

[43] M. Francesconi, S. Briola, M. Antonelli, A Review on Two-Phase Volumetric Expanders and Their Applications, Applied Sciences 12 (20) (2022) 10328, number: 20 Publisher: Multidisciplinary Digital Publishing Institute. doi:10.3390/app122010328.
URL https://www.mdpi.com/2076-3417/12/20/10328